Accepted for publication by the Astrophysical Journal
Preprint typeset using LaTeX style emulateapj v. 01/23/15

arXiv:1512.01164v2 [astro-ph.SR] 11 Dec 2015

TYPE IA SUPERNOVAE AND THEIR ENVIRONMENT: THEORY & APPLICATIONS TO SN 2014J

Paul Dragulin[1], Peter Hoeflich[2]

Accepted for publication by the Astrophysical Journal

ABSTRACT

We present theoretical semi-analytic models for the interaction of stellar winds with the interstellar medium (ISM) or prior mass loss implemented in our code SPICE [a], assuming spherical symmetry and power-law ambient density profiles and using the Π-theorem. This allows us to test a wide variety of configurations, their functional dependencies, and to find classes of solutions for given observations.

Here, we study Type Ia Supernova (SN Ia) surroundings of single and double degenerate systems, and their observational signatures. Winds may originate from the progenitor prior to the white dwarf (WD) stage, the WD, a donor star, or an accretion disk (AD). For M_{Ch} explosions, the AD wind dominates and produces a low-density void several light years across surrounded by a dense shell. The bubble explains the lack of observed interaction in late time SN light curves for, at least, several years. The shell produces narrow ISM lines Doppler shifted by 10-100 km/s, and equivalent widths of ≈ 100 mÅ and ≈ 1 mÅ in case of ambient environments with constant density and produced by prior mass loss, respectively. For SN 2014J, both mergers and M_{Ch} mass explosions have been suggested based on radio and narrow lines. As a consistent and most likely solution, we find an AD wind running into an environment produced by the RG wind of the progenitor during the pre-WD stage, and a short delay, 0.013 to 1.4 Myr, between the WD formation and the explosion. Our framework may be applied more generally to stellar winds and star-formation feedback in large scale galactic evolution simulations.

Subject headings: Supernovae: Type Ia: Circumstellar: Environment: Interaction : SN2014J

1. INTRODUCTION

Type Ia supernovae (SNe Ia) allow us to study the Universe at large and have proven invaluable in cosmological studies, the understanding of the origin of elements, and they are laboratories to study physics such as: hydrodynamics, radiation transport, non-equilibrium systems, nuclear and high energy physics. The consensus picture is that SNe Ia result from a degenerate C/O white dwarf (WD) undergoing a thermonuclear runaway (Hoyle & Fowler 1960), and that they originate from close binary stellar systems. Potential progenitor systems may either consist of two WD, the so called double degenerate system (DD), or a single WD along with a Main Sequence (MS) or Red Giant (RG) star, the so called single degenerate system (SD).

Within this general picture for progenitors, four classes of explosion scenarios are discussed which are distinguished by the mechanism which triggers the thermonuclear explosion: (1) Within the Chandraskhar mass M_{Ch} models, the explosion is triggered by compressional heat close to the center when the WD approaches M_{Ch}. The accretion material may originate either from a RG or MS companion via Roche-lobe overflow, or from tidal disruption of another WD in an DD system. (2) In a second class, the explosion is triggered by heat released during the dynamical merging (DM) of two WDs of a DD system. (In some cases, the combination may result in what is known as an accretion induced collapse). For overviews, see Branch et al. (1995); Nomoto et al. (2003); Di Stefano et al. (2011); Di Stefano & Kilic (2012); Wang & Han (2012); Hoeflich et al. (2013). (3) Recently, a third trigger mechanism has been revived known as double detonation scenario or He-detonation in a sub-M_{Ch} mass WD (Nomoto 1982a; Livne 1990; Woosley & Weaver 1994; Hoeflich & Khokhlov 1996; Kromer et al. 2010; Woosley & Kasen 2011). In this picture, a C/O WD star accretes He-rich material at a low rate to prevent burning. Explosions are triggered from ignition of the surface He layer with masses of about a few hundredths to 0.1 $M_\odot$. The resulting strong shock wave may trigger a detonation of underlaying C/O. Previous calculations produced a few $1/100^{th}$ $M_\odot$ of ^{56}Ni which is inconsistent with the early time spectra when the photosphere is formed within $10^{-3\cdots-2}M_\odot$ (Höflich et al. 1997). Modern recalculations have utilized a smaller He shell mass and obtain better agreement with observations (Kromer et al. 2010; Woosley & Kasen 2011), though, the problem with the outer layers still persists. Recent studies of helium detonations including curvature and expansion effects may be in better agreement with the observations (Moore et al. 2013; Ruiter et al. 2014; Zhou et al. 2014). For this class of explosions, we may expect accretion disk winds similar to those in M_{Ch} scenarios as discussed below. (4) Another explosion path, also recently set forth by Kashi & Soker (2011), is known as the core-degenerate (CD) scenario. They suggested that the merger between a WD and the hot core of an AGB star could take place within a common-envelope (CE) phase of binary evolution. The rotation of the core slows down by emitting magnetic dipole radiation until the angular momentum is insufficient to prevent collapse and susequent SN Ia. Binary/envelope interaction is expected to produce wind during a very short phase, similar to a planetary nebula (PN) mass loss phase.

[a] Supernovae Progenitor Interaction Calculator for parameterized Environments, available on request

[1] Department of Physics, Florida State University, Tallahassee, FL 32306, USA; pd09@my.fsu.edu
[2] Department of Physics, Florida State University, Tallahassee, FL 32306, USA; phoeflich77@gmail.com

It is not obvious that the properties would resemble a typical SNe Ia. Depending on the delay time from merging to explosion, the merged pair might explode within the PN shell or in a lower density ISM (Tsebrenko & Soker 2015).

The stellar environment will shed light on the evolutionary history of the progenitor, supernovae light curves (LCs), and spectra, with X-rays and radio emission being the probes (e.g. Chugai & Danziger (1994); Dwarkadas & Chevalier (1998); Chevalier & Irwin (2012); Chandra et al. (2012); Fransson et al. (2014)). As discussed below, the density limits for the environment of a typical SNe Ia are well below those of the solar neighborhood and one of the goals is to probe whether SD and/or DD systems may create this environment.

In the case of DD progenitors, we may expect long evolutionary time scales after the formation of the WDs compared to the accretion phase in M_{Ch} and the double detonation scenarios. The time scales depend on the unknown initial separation and mass of the binary WDs and the decay of the orbits due to gravitational waves (possibly modified during a common envelope phase). The time scale of angular momentum loss by gravitational waves scales with the fourth power of the separation (Landau & Lifshitz 1971). For example, the orbits of two 1 $M_\odot$ WDs at 1 $R_\odot$ will decay in $\approx 6 \times 10^8$ yr representing a period with no or little mass loss. However, we may expect wind just prior to the explosion when the WDs fill their Roche lobe. The size of the Roche lobe corresponds to a separation of $\approx 13,000$ km (Eggleton 1983) which translates to mass loss at most some months prior to the merging (Han & Webbink 1999), and material close to the system which will be quickly overrun by the SN material. In DD, therefore, we expect no ongoing wind with the exception of a brief period just prior to the dynamical merging. Thus, the environment of a DD system may be dominated by the ISM the system has moved into which depends on its peculiar velocity and the delay between WD formation and explosion. Mannucci et al. (2006) argued that the observed evidence of SNe Ia rates favors a bimodial distribution of the delay times between star formation and explosion with about 50 % of all explosions take place after ≈ 0.1 Gyr and 3 Gyr, respectively. Using the star formation rates and assuming that all SNe Ia originate from DD systems, Piersanti et al. (2009) concluded that 50 % of all DD systems explode within 4×10^8 yr, with a long tail to about 14 Gyr. Recent studies show that the distribution of delay times is more continuous (see Maoz et al. (2014) and references therein). It is likely that the DD system moved far away from its birthplace and that the explosion happens in the (constant density) ISM . In most cases, we may expect a low density environment consistent with observations.

The environment of SD systems can be expected to consist of three main components: 1) Some matter bound in the progenitor system at the time of the explosion that may originate from the accretion disk or be shed from the donor star; 2) the wind from the WD, accretion disk or donor star; and 3) the interstellar medium (ISM).

Within the scenario of M_{Ch} WD explosions, hydrodynamic calculations have shown that the expanding supernova ejecta wraps around the companion star and may pull off several tenths of a solar mass of material in case of a RG donor (Marietta et al. 2000; Kasen 2010). Besides the donor star, another source of matter is the accretion disk material (Gerardy et al. 2003) lifted during a pulsational phase during the explosion, or debris from the merging of two WDs (Hoeflich & Khokhlov 1996; Quimby et al. 2007a). There has been some observed evidence for interaction between the explosion and the immediate environment. Although H-lines like in SN 2002ic are rare, a common feature is a high-velocity $CaII$ line which, first, was prominently seen in events like SN1995D, SN 2001el, SN2003du, and SN 2000cx, a feature present in almost all SNe Ia (Hatano et al. 2000; Fisher 2000; Wang et al. 2003; Folatelli et al. 2013; Silverman et al. 2015). This line may be attributed to the material even of solar metallicity bound or in close proximity to the progenitor system [3]. (Gerardy et al. 2004; Quimby et al. 2007b).

At intermediate distances of up to several light years, in the case of M_{Ch} explosions, the environment may be dominated by the wind from the donor star, the accretion disk or, for high accretion rates, the wind from the WD, or the interstellar material (ISM). A number of possible interaction signatures has been studied, including X-rays, Radio, and narrow H and He lines, but no evidence has been found, with an upper limit of $10^{-5} M_\odot$ for the mass loss (Chugai 1986; Schlegel & Petre 1993; Schlegel 1995; Cumming et al. 1996; Chomiuk et al. 2012a). In late-time light curves, interaction should result in excess luminosity but, in general, is not seen. No sign of an interaction has been found even in SN1991T, which has been observed up to day 1000. This implies particle densities less than $\approx 10^{-3}$ cm^{-3}(Schmidt et al. 1994).

At large distances, from few tenths to several light years, the environment is determined by the ISM. It is known that Type Ia SNe generally explode away from star forming regions (Wang et al. 1997). This can be partly attributed to the long stellar evolutionary lifetimes of the low-mass stars in the progenitor systems, allowing them sufficient time to move away from their place of birth. It is also known that SNe Ia occur in elliptical and spiral galaxies, including galactic disks, the bulge and the halo. One may expect the explosion to occur in ISM particle densities of $\approx 10^{-3...1}$ cm^{-3} (Ferrière 2001). Light echos from SNe Ia have been used to probe their environments, and showed that many SNe Ia have circumstellar dust shells at distances ranging from a few up to several hundred parsecs (Hamuy et al. 2000; Rest et al. 2005; Aldering et al. 2006; Patat et al. 2007b; Crotts & Yourdon 2008; Wang et al. 2008; Rest et al. 2008).

Most evidence for a link between SNe Ia and their environment comes from the observations of narrow, time-dependent, blue-shifted NaID and KI absorption lines which, for a significant fraction of all SNe Ia, indicates outflows (D'Odorico et al. 1989; Patat et al. 2007a; Blondin et al. 2009; Foley et al. 2012; Sternberg et al. 2011; Phillips et al. 2013). In addition, extinction laws derived from SNe Ia seem to be different from the interstellar medium in our galaxy, suggesting a component linked to the environment of SNe Ia rather than the general host galaxy (Cardelli et al. 1989; Krisciunas et al. 2000; Elias-Rosa et al. 2006; Nordin et al. 2011; Pastorello et al. 2011). Possibly, the hydrodynamical

[3] H_α emission is suppressed by collisions, charge exchange and low ionization of hydrogen in absense of a strong, ongoing interaction with a Red Giant wind, see also Sect. 4.

impact of the SN ejecta will produce additional emission and may modify the outer structure of the envelope and, thus, the Doppler shift of spectra features. Light emitted from the photosphere of the supernovae may heat up matter in the environment, which, in turn may change the ionization balance or the dust properties (Raymond et al. 2013; Krügel 2015; Slavin et al. 2015; Patat et al. 2015a). We note that this effect for different dust formation in the host galaxy may lead to extinction laws different from the Milky Way as commonly observed in SNe Ia (Goobar 2008; Krisciunas et al. 2003; Folatelli et al. 2010; Kawara et al. 2011; Burns et al. 2014). The dust properties may effect the light echoes which could in turn change the extinction laws (Wang 2014).

The following picture of the environment emerges: SNe Ia are surrounded by a cocoon with a much lower environment than the ISM. Sometimes, narrow ISM lines indicate clumps or surrounding shells. However, the diversity of supernova and progenitor channels leaves open a huge parameter space which cannot be covered by numerical simulations. To cover the parameter space, we use a semi-analytic approach similar to those developed by Weaver et al. (1977) for stellar wind/ISM interaction, Chevalier & Imamura (1983) for stellar wind/stellar wind interaction, and Chevalier (1982) for supernova remnants. In our study, we make use of the Π theorem (Buckingham 1914; Sedov 1959) to study the classes of self-similar solutions for the environment of SNe Ia.

The current state of the research leaves some important questions unresolved. How can we understand the ubiquitously low density environment, their general structure, and their link to the progenitor systems? Do SNe Ia all originate from merging WDs? Which of the wide variety of progenitor systems are compatible with the observations and the range of parameters? What other possible signatures might be seen due to the interaction of the explosion within the possible progenitor systems? For SN 2014J, can we find a class of progenitor systems which is consistent with the lack of X-rays and radio (Margutti et al. 2014; Pérez-Torres et al. 2014), which favor dynamical merging scenarios, and the narrow ISM lines, which favor M_{Ch} mass explosions (Graham et al. 2015b)?

To address the questions, we developed a parameterized model in chapter 2 using fluid mechanics. In chapter 3, we present the application of semi-analytic models and our code SPICE as an analysis tool in the framework of environment of SNe Ia. We evaluate the imprint of different environments and wind properties. In chapter 4, we apply the framework to SN 2014J as an example (see Fig. 17) and discuss the results. In chapter 5, final discussions and conclusions are presented.

2. THEORY AND ASSUMPTIONS

We develop here a model for wind-environment interaction from basic fluid mechanics. In the case of spherical symmetry and adiabatic flows, the hydrodynamic equations take the form:

$$\frac{\partial \rho}{\partial t} + \frac{1}{r^2}\frac{\partial}{\partial r}(r^2 \rho u) = 0 \tag{1}$$

$$\frac{\partial u}{\partial t} + u\frac{\partial u}{\partial r} + \frac{1}{\rho}\frac{\partial p}{\partial r} = 0 \tag{2}$$

$$\frac{\partial p}{\partial t} + u\frac{\partial p}{\partial r} + \frac{\gamma p}{r^2}\frac{\partial}{\partial r}(r^2 u) = 0 \tag{3}$$

where u is the fluid velocity, ρ is the mass density, p is the pressure, and $\gamma = 5/3$ is the adiabatic index. The structures have four characteristic regions (Fig. 1): I) undisturbed wind emanating from the source between $r = 0$ and an inner shock front R_2, II) the inner shocked region of accumulated wind matter between R_2 and the contact discontinuity $R_{\rm C}$, III) an outer region of swept-up interstellar gas between $R_{\rm C}$ and the outer shock R_1, and IV) the outermost, undisturbed, ambient medium.

The solutions for regions I and IV are trivial. The solution for region III was found by Parker (1963) who implimented a self-similar ansatz and the following transformations:

$$u = \frac{r}{t}U(\eta) \tag{4}$$

$$\rho = \Omega(\eta)\rho_c r^{-s} \tag{5}$$

$$p = r^{2-s}t^{-2}\rho_c P(\eta) \tag{6}$$

$$\eta = t r^{-\lambda} \tag{7}$$

where $\rho_0(r) = \rho_c r^{-s}$ for the outer density. The similarity exponent λ can be found by dimensional analysis.

$$R_{\rm C} \propto (\dot{m} {v_w}^2/2)^{\alpha} (\rho_c)^{\beta} t^{1/\lambda} \tag{8}$$

$\lambda = 5/3$ for $s = 0$ and $\lambda = 1$ for $s = 2$ (See Eqs. 16 and 24 for exact expressions of $R_{\rm C}$). Substituting these into equations 1, 2 and 3, making the substitution $\chi = \gamma\frac{P(\eta)}{\Omega(\eta)}$, and re-arranging gives us the following:

$$\frac{d\chi}{d\log(\eta/\eta_1)} = \frac{\gamma\chi(1-\lambda U)[2 + U(1 - 3\lambda - 3\gamma + \lambda\gamma) + 2\lambda\gamma U^2] + \lambda\chi^2(s\gamma - 2\gamma + 2 - s - 2\lambda + 2\lambda\gamma U)}{\gamma(1-\lambda U)[(1-\lambda U)^2 - \lambda^2\chi]} \tag{9}$$

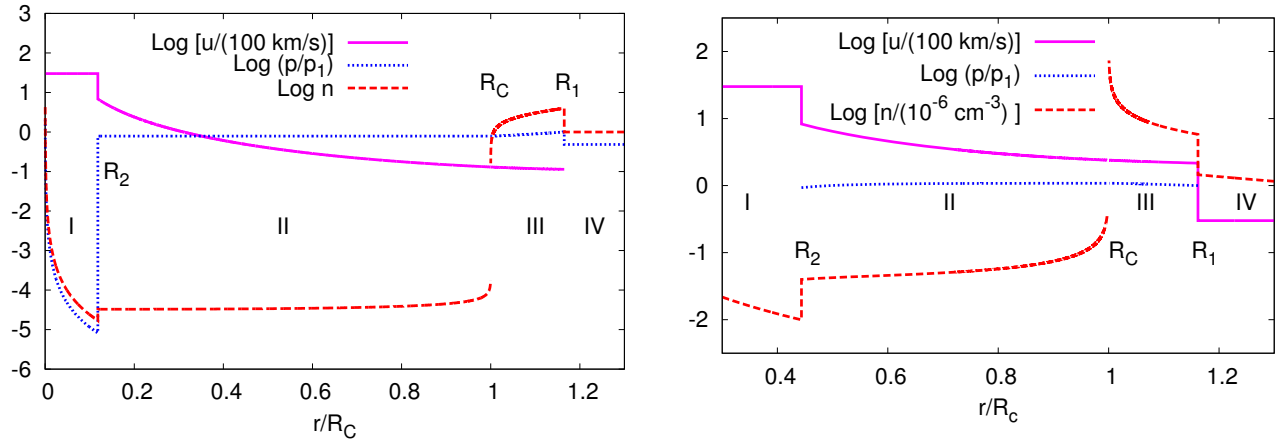

FIG. 1.— Velocity, pressure and density structure of a typical model shows four distinct regions dominated by the wind (I), the reversed shock (II), a shell (III), and the environment (IV) both for constant density environments (left) and environments produced by prior mass loss (right). In the figures of this work, density is shown in particle density $n = \rho N_A/\overline{\mu}$, where N_A is Avogadro's number and $\overline{\mu}$ is the mean molecular weight. In this work, $\overline{\mu}$ is set equal to 1. For different $\overline{\mu}$, $\rho \rightarrow \overline{\mu}\rho$ in all equations.

$$\frac{dU}{d\log(\eta/\eta_1)} = \frac{\gamma U(1-U)(1-\lambda U) + \chi(2\lambda + s - 2 - 3\lambda\gamma U)}{\gamma(1-\lambda U)^2 - \gamma\lambda^2\chi} \tag{10}$$

$$\frac{d\log(P/P_1)}{d\log(\eta/\eta_1)} = \frac{2 + U(s - 2 - 2\lambda + \lambda\gamma - 3\gamma) + \lambda U^2(2 - s + 2\gamma) + \lambda\chi(s-2)}{(1-\lambda U)^2 - \lambda^2\chi} \tag{11}$$

The outer boundary conditions are obtained from the Rankine-Hugoniot jump conditions for large Mach numbers:

$$\chi_1 = \frac{2\gamma(\gamma-1)}{\lambda^2(\gamma+1)^2} \tag{12}$$

$$P_1 = \frac{2}{\lambda^2(\gamma+1)} \tag{13}$$

$$U_1 = \frac{2}{\lambda(\gamma+1)}. \tag{14}$$

Integration is carried out with respect to U from the outer shock R_1 where $U = U_1$ to the contact discontinuity R_C where the velocity u is equal to $dR_C/dt = \frac{R_C}{\lambda t}$ and hence $U_c = 1/\lambda$.

The solution for region III is self-similar because the only relevant parameters are the mechanical luminosity of the wind $\frac{1}{2}\dot{m}{v_w}^2$ emanating from the origin and the outer density constant ρ_0. There is no way to obtain a parameter with dimension of length or time using those parameters. This is not the case in region II, where the relevant parameters are ρ_c, as well as $\dot{m}$ and v_w, individually. Therefore, in the case of $s = 0$ a self-similar solution is not possible in region II, as was shown by Weaver et al. (1977). They did however obtain useful analytic relations directly from the hydrodynamic equations by assuming that region II was isobaric. Their results for the locations of the inner shock, contact discontinuity, outer shock, the velocity, pressure, and density are the following:

$$R_2(t) = 0.748\,(\dot{m}/\rho_0)^{3/10}\, v_w^{1/10} t^{2/5} \tag{15}$$

$$R_C(t) = 0.660\,\left(\dot{m}v_w^2/\rho_0\right)^{1/5} t^{3/5} \tag{16}$$

$$R_1(t) = 0.769\left(\frac{\dot{m}v_w^2}{\rho_0}\right)^{1/5} t^{3/5} \tag{17}$$

$$u(r,t) = \frac{11}{25}\frac{R_C(t)^3}{r^2 t} + \frac{4}{25}\frac{r}{t} \tag{18}$$

$$p(t) = 0.126\,\left(\dot{m}^2 v_w^4 \rho_0^3\right)^{1/5} t^{-4/5} \tag{19}$$

$$\rho(r,t) = 0.628\left(\frac{\dot{m}^2\rho_0^3}{v_w^6}\right)^{1/5} t^{-4/5}\left(1 - \frac{r^3}{R_C(t)^3}\right)^{-8/33} \tag{20}$$

after correcting a small typographical error in their given expression for the velocity. This is the solution for the structure of the interaction region for the $s = 0$ (constant IS density) case as the Mach number goes to infinity.

One notable feature about these structures is that the density goes to zero as r approaches $R_{\rm C}$ from above but diverges to infinity upon approach from below. Pressure and fluid velocity are finite and continuous across the boundary. Using the analytic expression for $\rho(r)$ (equation 20) we may define a characteristic width of the density peak in the inner region by $\Delta r_\rho \equiv R_{\rm C} - r(2\rho_2) = R_{\rm C}[1 - 2^{-33/8}(1 - {R_2}^3/{R_{\rm C}}^3)]^{1/3}$, where $r(\rho)$ is the inverse of equation $\rho(r)$ as given in 20. The width of region III is given by the integration of the equations 9 and 10; it is $\Delta r_{III} = 0.165 R_{\rm C}$. The temperature varies with the inverse of the density. In reality the extreme temperature discontinuity will smooth out due to finite heat conduction.

2.1. *Self-similar solutions for s=2*

The case for $s = 2$ allows us self-similar solutions because all characteristic scales R are proportional to t (Eq. 8) and, thus, the time-dependence cancels out. Chevalier & Imamura (1983) found self similar solutions for the interaction regions of colliding winds. Their work is similar to what we do here. The density in region IV is of the form $\rho_0(r) = \frac{\dot{m}_1}{4\pi v_{w,1} r^2}$ assuming it is of a prior stellar wind with parameters $\dot{m}_1$ and $v_{w,1}$. The boundary conditions become

$$\chi_i = \frac{2\gamma(\gamma-1)}{(\gamma+1)^2}\left(\frac{v_{w,i}t}{R_i} - 1\right)^2 \tag{21}$$

$$P_i = \frac{2}{\gamma+1}\left(\frac{v_{w,i}t}{R_i} - 1\right)^2 \tag{22}$$

$$U_i = \frac{1}{\gamma+1}\left[2 + (\gamma-1)\frac{v_{w,i}t}{R_i}\right] \tag{23}$$

where the subscript i is either 1 or 2, referring to the outer and inner shock front boundaries, respectively ($v_{w,2} = v_w$). Using the Buckingham Pi theorem (Buckingham 1914; Sedov 1959), we obtain the following expression for $R_{\rm C}$:

$$R_{\rm C} = K_{2C}(\Pi_{\dot{m}}, \Pi_{v_w}) v_w t \tag{24}$$

$$R_1 = K_{21}(\Pi_{\dot{m}}, \Pi_{v_w}) v_w t \tag{25}$$

$$R_2 = K_{22}(\Pi_{\dot{m}}, \Pi_{v_w}) v_w t \tag{26}$$

with

$$\Pi_{\dot{m}} = \dot{m}/\dot{m}_1 \tag{27}$$

$$\Pi_{v_w} = \frac{v_w}{v_{w,1}} - 1. \tag{28}$$

$K_{2C,1,2}$ are functions to be determined numerically. By requiring pressure continuity across $R_{\rm C}$, we acquire an analytic expression for the inner shock radius as a function of time:

$$R_2 = v_w t\left[1 + \left(1 - \frac{t v_{w,1}}{R_1}\right)\sqrt{\left(\frac{P_2}{P_c^-}\right)\left(\frac{P_c^+}{P_1}\right)\frac{\rho_{c,1}}{\rho_{c,2}}}\right]^{-1}. \tag{29}$$

The outer shock radius can be given by

$$R_1 = (\eta_c^+/\eta_1)(\eta_2/\eta_c^-) R_2, \tag{30}$$

and likewise

$$R_{\rm C} = (\eta_1/\eta_c^+) R_1. \tag{31}$$

The quantities (P_2/P_c^-), (P_c^+/P_1), (η_c^+/η_1) and (η_c^-/η_2) are found from integrating equations 9, 10 and 11 in either region III (+) or II (−). However, in order to calculate them, initial guesses of R_1, R_2 and $R_{\rm C}$ are required. A consistent solution is obtained by damped fixed-point iteration. As Fig. 1 shows, the structures are qualitatively different for $s = 2$ than for when $s = 0$. The density goes to infinity as one approaches $R_{\rm C}$ from either side while the pressure is finite. Formally, the temperature therefore goes to zero.

TABLE 1
For constant ISM and $t \lesssim t_p$, the relations for the radius of the contact discontinuity R_C, the forward and reverse shock, R_1 and R_2, the fluid velocity at the shell u_c, its mass column density τ_m, and the density of the inner void, n_2, all as a funciton of the density of the environment n_0, the mass loss $\dot{m}$, its wind velocity v_w, and duration t. For n_2, we assumed $(R_2/R_C)^3 \ll 1$ (see Eq. 20). Asymptotic ($t \to \infty$) values of the reverse shock $R_{2,\infty}$, and the particle density $n_{2,\infty}$ are obtained from the FAP model and given below. p_0 is the ambient pressure.

R_C	$\propto$	$n_0^{-\frac{1}{5}} v_w^{\frac{2}{5}} \dot{m}^{\frac{1}{5}} t^{\frac{3}{5}}$
R_1	$\propto$	$n_0^{-\frac{1}{5}} v_w^{\frac{2}{5}} \dot{m}^{\frac{1}{5}} t^{\frac{3}{5}}$
R_2	$\propto$	$n_0^{-\frac{3}{10}} v_w^{\frac{1}{10}} \dot{m}^{\frac{3}{10}} t^{\frac{2}{5}}$
u_c	$\propto$	$n_0^{-\frac{1}{5}} v_w^{\frac{2}{5}} \dot{m}^{\frac{1}{5}} t^{-\frac{2}{5}}$
n_2	$\propto$	$n_0^{\frac{3}{5}} v_w^{-\frac{6}{5}} \dot{m}^{\frac{2}{5}} t^{-\frac{4}{5}}$
τ_m	$\propto$	$n_0^{\frac{4}{5}} v_w^{\frac{2}{5}} \dot{m}^{\frac{1}{5}} t^{\frac{3}{5}}$
t_p	$\propto$	$n_0^{\frac{3}{4}} v_w \dot{m}^{-\frac{1}{2}} p_0^{-\frac{5}{4}}$
$R_{2,\infty}$	$\approx$	$0.30\sqrt{\frac{\dot{m} v_w}{p_0}}$
$n_{2,\infty}$	$\approx$	$3.9\ p_0/v_w^2$

2.2. *Self-similar Solutions for s=0 and Boundary Conditions*

As discussed above, the self-similar solution depends on the ambient density, ρ_0, and the kinetic energy flux, $1/2\,\dot{m}{v_w}^2$ at the inner boundary. For constant density ISM (s=0), the solutions are not valid for $t \to 0$ and $t \to \infty$. This is because physical assumptions break down and the results are unphysical solutions.

For small times, this can be seen as follows: As shown in Table 1, $R_C \propto t^{3/5}$ and $R_2 \propto t^{2/5}$. This implies the velocity of the reverse shock would go against infinity. No interaction is possible if the wind cannot overrun R_2, therefore the description becomes unphysical. Also, the reverse shock R_2 is greater than the contact discontinuity R_C for small enough t. Therefore, no self-similar solutions exist for $\dot{R}_2 \approx v_w$ and $R_2 \approx R_C$, i.e. times shorter than $t \sim \sqrt{\frac{\dot{m}}{\rho_0 {v_w}^3}}$. For our application to SN environments at times greater than when interaction takes place within the progenitor system, this hardly poses a limitation. For our reference model in the accretion disk wind case, the MS wind, and the RG-like wind (see tables 3,4 & 5) the critical times are 3.8 yr, 0.17 yr, and 1.2×10^4 yr, respectively. The times where no self-similar solutions exist are short compared to the duration of the winds from the progenitor system.

For large times, the solution depends on the outer boundary condition, namely the pressure of the ambient medium. In the following, we want to consider the validity of solutions at large times, and develop approximations which allow us to study environmental properties. We will compare solutions with and without ambient pressure. We will refer to those as zero-ambient pressure (ZAP) and finite-ambient pressure models (FAP), respectively.

For $t \to \infty$, R_C goes out indefinitely according to the self-similar solution as external pressure is neglected. In reality, the outer pressure will increasingly confine the expansion of the structure and, thus, R_C. In the self-similar solution without ambient pressure, p_1 decreases with ${R_1}^2/t^2 \propto t^{-4/5}$ (Eq. 39) and, eventually, it will drop below the ambient pressure of the physical medium. As reference, we define the pressure-equilibration time t_p as the time at which the pressure just inside R_1 equals the ambient (constant) pressure, p_0. It is given by

$$t_p = 1.23\sqrt{\frac{\dot{m}{v_w}^2}{\rho_0}} \times \left[\lambda^2(\gamma+1)\frac{p_0}{\rho_0}\right]^{-5/4}. \tag{32}$$

In Fig. 2, we give the evolution of the basic physical quantities as a function of time for models with parameters typically for AD-, RG-like and MS-star winds. For our reference models (see Tables 3, 4 and 6), assuming an ideal gas ambient pressure given by temperature $T_0 = 10^4$ K, we obtain in the AD wind case, the RG-like wind, and the MS wind $t_p = 7.45 \times 10^5$ yr, $t_p = 2.36 \times 10^5$ yr, $t_p = 124$ yr, respectively.

As an extreme case and benchmark for modifications, we use a MS wind with parameters similar to the Sun and an evolutionary time $t = 4 \times 10^7 yr$ (see reference model in Table 6). t_p is some 124 years only, i.e. smaller than t by a factor of 3×10^5. In the ZAP model, the contact discontinuity R_C and the location of the reversed shock are about 23 and 20 ly, respectively. The solar wind has similar properties but the termination shock is at about 75 to 95 AU based on Voyager 1 (Shiga 2007). The discrepancies can be understood due to the ambient pressure not being taken into

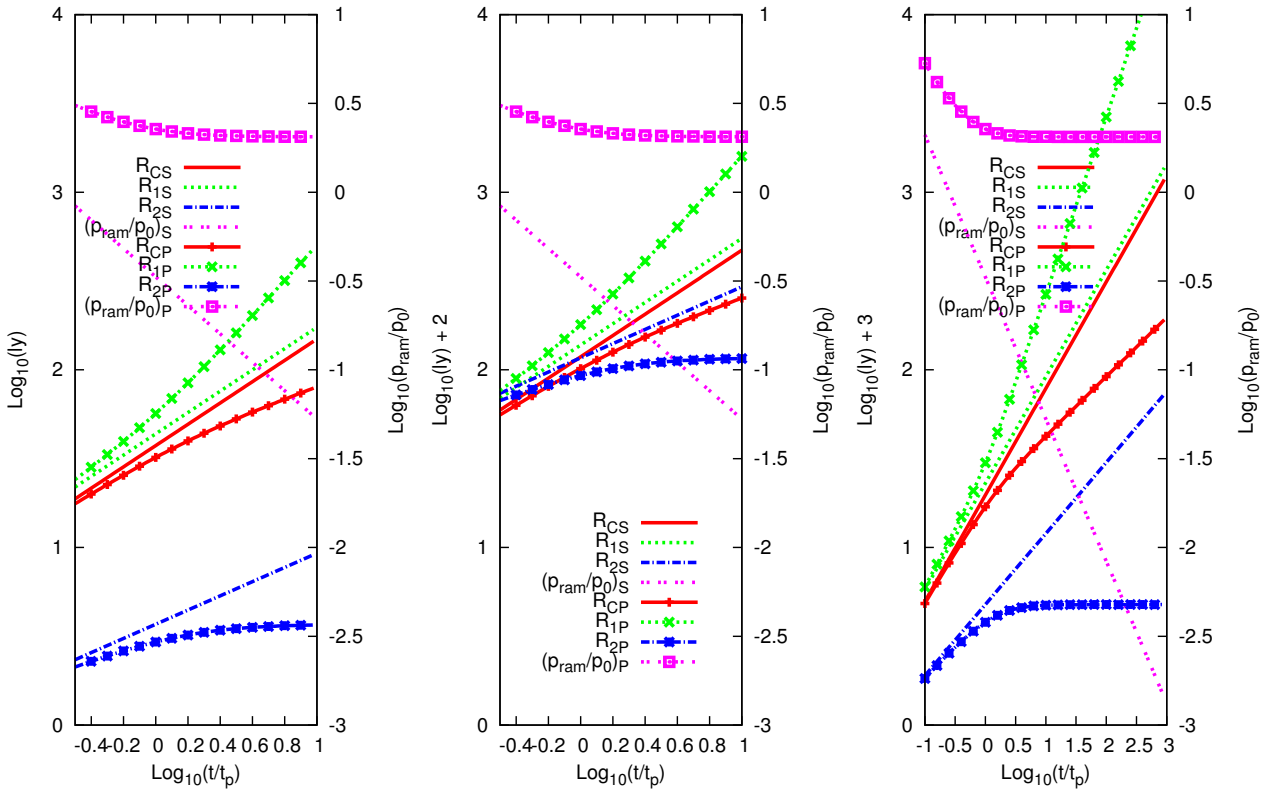

FIG. 2.— Structure feature comparisons of ZAP and FAP models for given sets of parameters as a function of t/t_p for the reference models of the AD-, RG-like and MS wind (right to left). Dependence of the radii of the outer and inner shock $R_{1,2}$, of the contact discontinuity R_C, and the ram pressure p_{ram}/p_0 are shown as a function of the duration of the wind t normalized to the time t_p at which the inner and outer pressure are equal. We show the functions for the zero ambient and finite pressure model indicated by the small and large symbols, respectively.

account. Moreover, for times much larger than t_p, $\dot{R_C} \ll c_s$ where c_s is the ambient sound speed. We would therefore expect turbulent instabities which results in mixing. Ignoring ambient pressure for the MS (solar) model results in the contact discontinuity overrunning the the heliopause in about 10 years. Therefore, it is imperative that we consider how to account for finite ambient density in order to get realistic solutions.

A first order estimate for the solution may be obtained by stopping the time integration at t_p for a model without ambient pressure, and neglecting the further evolution. For R_C and R_2 and with this crude approximation, we obtain the right order of magnitude with $R_2 = 190\ AU$ compared to the solar value of 75 to 95 AU.

In the following, we will construct physically motivated boundary conditions for moderate $log(t/t_p) < 1 \ldots 3$, and discuss the uncertainties estimated by a comparison between the finite ambient pressure model (FAP) and zero ambient pressure model (ZAP).

Besides simply truncating the solution at t_p, there is a way to approximately incorporate the ambient pressure in a way that retains the self similar solution at any time, although with a modified ambient pressure profile. In order to see how, we first notice the Rankine-Hugoniot jump conditions (in shock rest frame):

$$p' = \frac{2\rho_0 {u_0}^2 - (\gamma - 1)p_0}{\gamma + 1} \tag{33}$$

$$u' = \frac{2\gamma p_0 + (\gamma - 1)\rho_0 {u_0}^2}{(\gamma + 1)\rho_0 u_0} \tag{34}$$

$$\rho' = \frac{(\gamma + 1){\rho_0}^2 {u_0}^2}{2\gamma p_0 + (\gamma - 1)\rho_0 {u_0}^2} \tag{35}$$

where the 0 subscripts denote pre-shock and the primed variables are post-shock quantities. After applying the substitutions in 4, 5, and 6, we see that the boundary conditions can remain constant with respect to space and time if p_0 follows a spacial power law with $r^{-4/3}$ (or, equivalently, a time power-law of $t^{-4/5}$. This is because $R_1 \propto t^{3/5}$.). An effective pressure power law environment can be defined by requiring that, at a certain final time t_f, the thermal energy contained within $R_1(t_f)$ in our effective environment is equal to the thermal energy in the physical, constant

ambient density at the same radius. We find it by volume integration along $R_1(t)$: $p_{\rm eff}(t) = \frac{5p_0}{9}\left(\frac{t_f}{t}\right)^{4/5}$. Although t_f can be thought of as a constant parameter used to define the environment, in practice $t_f = t$ and $p_{\rm eff}(t) = \frac{5p_0}{9}$. However, we note that, as the solution advances forward in time, this means that t_f and the boundary condition will vary as well, meaning the solution will not be truly "self-similar," ie the morphology changes with time. The solution obtained in this way is, in fact, a series of snapshots of self-similar solutions where t_f is equal to the instantaneous time t. Using this parameterisation, the Buckingham Π theorem gives us the following:

$$R_{\rm C} = K_{0\rm C}\left(\Pi_0\right)\left(\frac{\dot{m}v_w^2t^3}{\rho_0}\right)^{1/5} \tag{36}$$

$$R_1 = K_{01}\left(\Pi_0\right)\left(\frac{\dot{m}v_w^2t^3}{\rho_0}\right)^{1/5} \tag{37}$$

$$\Pi_0 = \left(\frac{\dot{m}v_w^2}{\rho_0(R_sT_0)^{5/2}t^2}\right)^{1/5} \tag{38}$$

where the Ks are to be determined numerically and the ideal gas relation was used: R_s is the gas constant divided by the mean molecular weight and T_0 is the physical ambient, constant temperature. T_0 will be taken to be 10^4 K typical for ISM gas (Osterbrock & Ferland 2006). Note that, using Eqs 38 and 32 (for $\gamma = 5/3$), we have $\Pi_0 = 2.50(t/t_p)^{-2/5}$.

The outer boundary conditions of the ODEs are then given as:

$$\chi_1 = \frac{(2\gamma - (\gamma-1)/M^2)(2/M^2+\gamma-1)}{\lambda^2(\gamma+1)^2} \tag{39}$$

$$P_1 = \frac{(2\gamma - (\gamma-1)/M^2)}{\lambda^2\gamma(\gamma+1)} \tag{40}$$

$$U_1 = 2\frac{1-1/M^2}{\lambda(\gamma+1)} \tag{41}$$

where the Mach number M is given by:

$$M = \frac{R_1(t)}{\lambda t}\sqrt{\frac{9\rho_c}{5\gamma p_0}}. \tag{42}$$

An initial guess of R_1 is required in order to numerically solve the ODEs and obtain the structure, therefore iteration is necessary in order to obtain a consistent solution. Following the method of Weaver et al. (1977) using with our modified boundary conditions, we obtain the following expressions for the radii and inner structure profile:

$$R_2(t) = 1.13(\beta\alpha)^{3/2}\left(\frac{\dot{m}}{\rho_0}\right)^{3/10}{v_w}^{1/10}t^{2/5} \tag{43}$$

$$R_1(t) = \alpha/2^{1/5}\left(\frac{\dot{m}{v_w}^2}{\rho_0}\right)^{1/5}t^{3/5} \tag{44}$$

$$R_{\rm C}(t) = \beta R_1 \tag{45}$$

$$u(r,t) = \frac{11}{25}\frac{{R_{\rm C}}^3}{r^2t} + \frac{r}{25t} \tag{46}$$

$$p(r,t) = \frac{5}{22\pi(\beta\alpha)^3}(1/4\dot{m}^2{v_w}^4{\rho_0}^3)^{1/5}t^{-4/5} \tag{47}$$

$$\rho(r,t) = \frac{0.274}{(\alpha\beta)^3}\left(\frac{\dot{m}^2{\rho_0}^3}{{v_w}^6}\right)^{1/5}t^{-4/5}\left(1-\frac{r^3}{{R_{\rm C}}^3}\right)^{-8/33} \tag{48}$$

where $\alpha = \frac{1}{\beta}\left(\frac{5}{22\pi P_c^+}\right)^{1/5}$, $\beta = \left(\frac{\eta_c}{\eta_1}\right)^{-1/\lambda}$, and P_c^+ and η_c are evaluated at the contact discontinuity. Comparison of eqs. 44, 45 with eqs. 37, 36 give $K_{01} = \frac{\alpha}{2^{1/5}}$ and $K_{0\rm C} = \frac{\beta\alpha}{2^{1/5}}$. We can then define a proportionality for the reverse shock:

$$R_2 = K_{02}(\Pi_0)\left(\frac{\dot{m}}{\rho_0}\right)^{3/10}v_w^{1/10}t^{2/5} \tag{49}$$

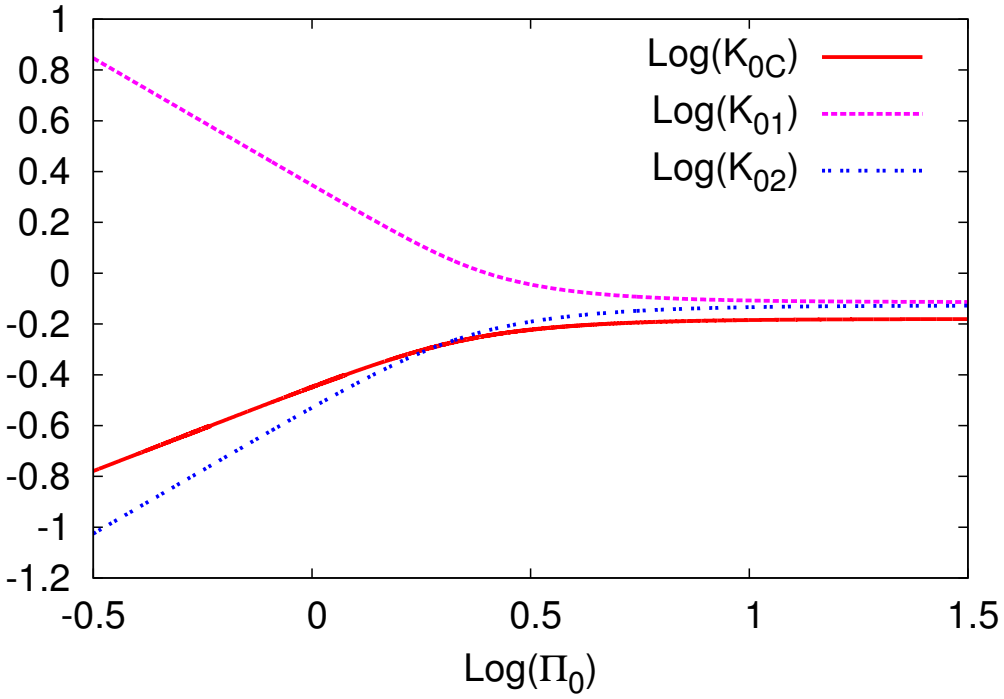

FIG. 3.— Proportionality factors for the characteritic distances as a function of Π_0 for constant density environments and the FAP model. Note that all factors are constant for ZAP models with values corresponding to large Π_0 (see Sect.2).

where

$$K_{02} = 1.39 K_{0C}^{3/2}. \tag{50}$$

For $p_0 \to 0$, $M \to \infty$, $\alpha \to 0.88$, $\beta \to 0.86$, and eqns 15-20 from the last section are reproduced. For the reference models for an AD-, RG-like and MS-wind, a comparison of the basic properties between the ZAP and FAP models as a function of t/t_p is shown in Fig. 2. Qualitatively, the main differences are as follows: For FAP models, R_2 and R_C are smaller and R_1 is larger than for ZAPs, and R_2 goes to a constant value for large t/t_p. For the range shown and for the RG-like wind, R_2 becomes larger than R_C at about $log(t/t_p) \approx -0.5$ marking the regime of "unphysical" solutions already discussed above for the ZAP model. The functional relations appear to be similar and, in fact, they are identical as a consequence of the Π theorem. The relative shifts between the various quantities are given by proportionality factors which, in turn, depend only on the basic parameters, namely v_w, $\dot{m}$ and n_0. For the FAP model, the proportionality constants have to be determined numerically (Fig. 3). A further consequence of the Π theorem is that the differences are only a function of t/t_p and do not depend individually on $\dot{m}$, v_w and n_0 (Fig. 4). For a constant density medium, the characteristic parameters can be directly obtained using Fig. 3.

The detailed solutions for our reference models are shown in Figs. 5 & 6. The morphology of the envelopes does not change for a wide range of parameters and time. As discussed above in case of the MS star wind, however, we must expect strong mixing for $t/t_p \gg 1$ in FAP models. The solution becomes "un-physical" for $r \gtrsim R_C$ in the regime of a weak shock.

2.3. *Existence of Solutions*

Here, we want to provide the range for which self-similar solutions exists using the Π theorem.
Case I (s=0) : For FAP and s=0, there is one Π group given by Eq 38. Solutions do not exist for Mach numbers less than 1.3849.
Case II (s=2): Two Π groups exist and, thus, possible solutions are a combination of Π groups with $K_2(\Pi_{\dot{m}}, \Pi_{v_w})$ given by equations 27 and 28. For r^{-2} ambient density profiles, the shell velocity range is sufficient to determine the relation between $\dot{m}_1$ and $v_{w,1}$ for the prior mass loss. In Figs. 7, 8 & 9, we show K_{2C}, K_{21} and K_{22} as a function of the wind parameters covering the entire range discussed in this paper.

Regime I: For high mass loss rates, we have no power law relation between the wind and environmental parameters, and the values of K_{2C}, K_{21} and K_{22} need to be interpolated in the figures or can be calculated by SPICE.

Regime II: If a low mass loss wind runs into a high mass loss wind, $\Pi_{\dot{m}} < 0.1$, K_{2C}, K_{21}, K_{22} hardly vary with the ratio $\dot{m}/\dot{m}_1$. Thus, the contour lines in Figs. 7, 8 & 9 are horizontal. Their value can be approximated therefore as a function of only the relative wind velocities. In Fig. 10, the variation of the cuts for various $\Pi_{\dot{m}}$. K_{2C} and K_{21} can be well described by single functions. K_{22} needs two descriptions valid at low and high ratios of $v_w/v_{w,1}$ separated at

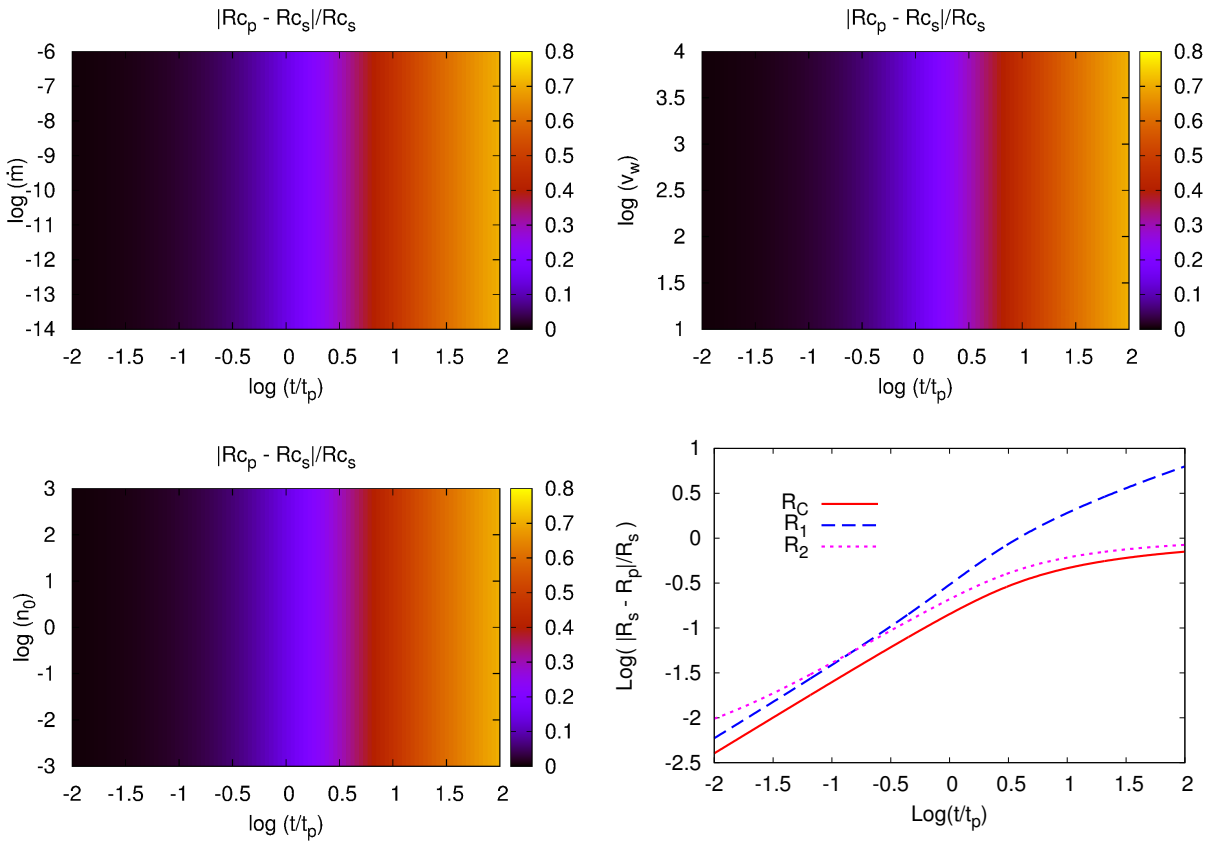

FIG. 4.— Fractional difference in R_C between models of zero ambient pressure ($R_{C,s}$) and finite pressure models ($R_{C,p}$) in the parameter space of the mass loss $\dot{m}$, the wind velocity v_w, and the environment density n_0 as a function of $log(t/t_p)$. The plots visualize the Π-theorem as discussed in Sect. 3: The difference depends on (t/t_p) only. The ratios between scale-free variables are constant throughout the parameter space. The Π-theorem applies also to R_1. In the lower right, we show the fractional difference of R_C (red), R_1 (blue) and R_2 (magenta) between the ZAP and FAP models as a function of $log(t/t_p)$.

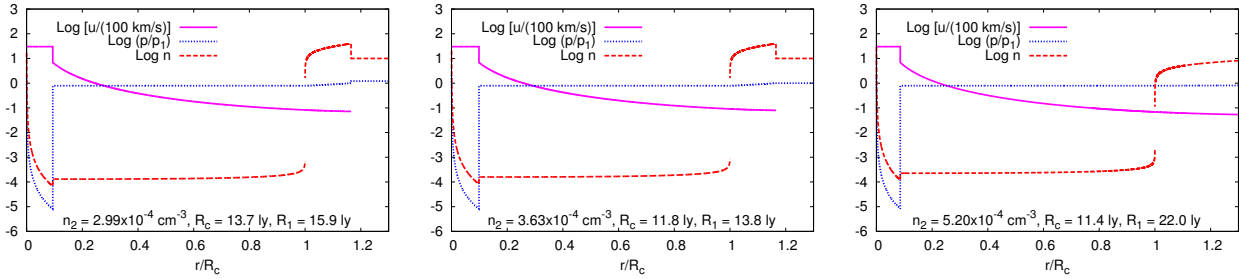
Log [u/(100 km/s)]
Log (p/p_1)
Log n
n_2 = 2.99x10^-4 cm^-3, R_c = 13.7 ly, R_1 = 15.9 ly
r/R_c
Log [u/(100 km/s)]
Log (p/p_1)
Log n
n_2 = 3.63x10^-4 cm^-3, R_c = 11.8 ly, R_1 = 13.8 ly
r/R_c
Log [u/(100 km/s)]
Log (p/p_1)
Log n
n_2 = 5.20x10^-4 cm^-3, R_c = 11.4 ly, R_1 = 22.0 ly
r/R_c

FIG. 5.— Structure of model 3 for AD wind (see Table 3). We show the ZAP (left) with $t = 3 \times 10^5$ yr and at $t = t_p$ (middle), and the FAP model at $t = 3 \times 10^5$ yr. The overall structure is similar within the parameter range.

Log $\Pi_{v_w} \approx 0.5$. The resulting power law dependencies are given in Table 2.

3. APPLICATIONS: ENVIRONMENTS OF TYPE IA SUPERNOVAE PROGENITORS

We will explore winds emanating from the progenitor system and interacting with the ISM of mass loss of the system prior to the supernova explosion. We consider winds from each source separately, and we address the question of which component is mostly responsible for the formation of the environment, and the typical structure to be expected. Subsequently, we discuss the link between observables and progenitor systems, and analyze SN 2014J.

We employ our spherical, semi-analytical models constructed by piecewise, scale-free analytic solutions. Scales enter the system via the equation of state, the boundary, and the jump conditions. The free parameters are: 1) The velocity v_w, 2) mass loss rate $\dot{m}$ from the central object, and the 3) $n_0 = const$ or a mass loss rate $\dot{m}_1$ with $v_{w,1}$, i.e. $n \propto r^{-s}$, and 4) the duration of the wind interaction t. As a result, we obtain the density, velocity and pressure as a function of time, namely $\rho(r,t), v(r,t)$ and $p(r,t)$ which can be linked to observables. We use typical parameters to discuss the

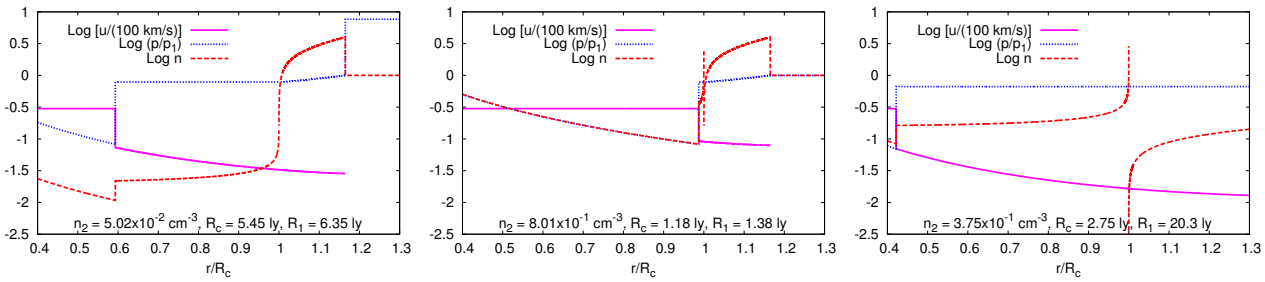
Log [u/(100 km/s)]
Log (p/p1)
Log n
n2 = 5.02x10-2 cm-3, Rc = 5.45 ly, R1 = 6.35 ly
n2 = 8.01x10-1 cm-3, Rc = 1.18 ly, R1 = 1.38 ly
n2 = 3.75x10-1 cm-3, Rc = 2.75 ly, R1 = 20.3 ly
r/Rc

FIG. 6.— Same as Fig. 5 but for RG-like winds (see Table 4).

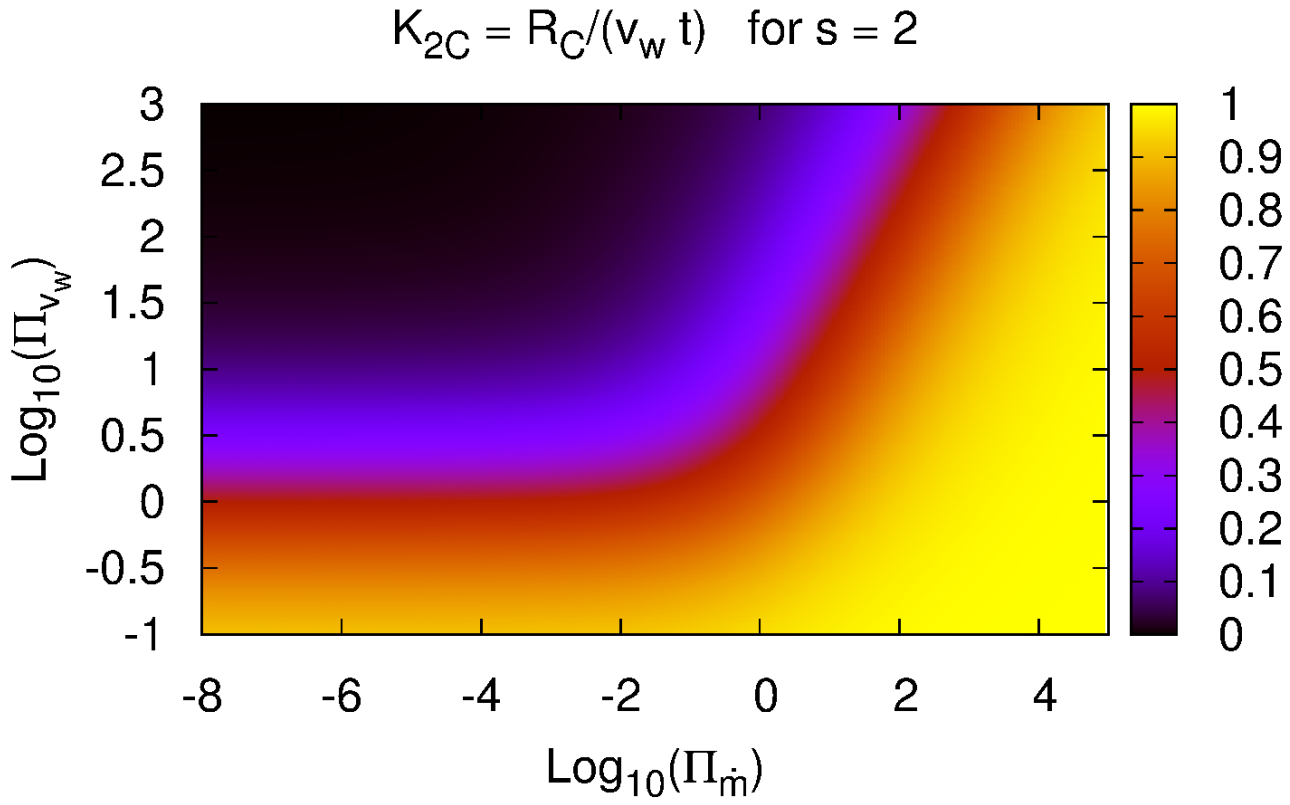

FIG. 7.— Value of K_{2C} as a function of v_w and $\log K_2(\Pi_{\dot{m}}, \Pi_{v_w})$ where $\Pi_{v_w} = (v_w - v_{w,1})/v_{w,1})$ and $\Pi_{\dot{m}} = (\dot{m}/\dot{m}_1)$. K_{2C} is close to constant in the regime of low mass winds running into high mass loss wind, i.e. $log(\Pi_{\dot{m}}) < 0$.

different regimes which may occur in nature. For actual fits of observations, appropriate solutions can be constructed by tuning these parameters with SPICE.

The wind may originate from the AD, the donor star which may be a MS or a RG-, horizontal- and asymptotic-branch star, the WD during a phase of over-Eddington accretion, or a combination of AD with a RG-like wind. As shown below, the time scale for the accretion and, thus, the progenitor, is an important factor in formation of the environment. The time scales t vary widely depending on the scenario and chemical composition of the accreted material and the initial mass of the progenitor (e.g. (Sugimoto & Nomoto 1980; Piersanti et al. 2003a; Wang & Han 2012) and reviews cited in the introduction). To reach M_{Ch}, about 0.2 to 0.8 $M_\odot$ of material needs to be accreted. For hydrogen accretion, the rates for stable hydrogen burning are between $\dot{M} \approx 2 \times 10^{-8\cdots-6}\ M_\odot/yr$ depending on the metallicity (Nomoto 1982b; Hachisu et al. 2010). The upper and lower limits for $\dot{M}$ are set by the Eddington limit for the luminosity and the minimum amount of fuel needed for steady burning, respectively. However, it is under discussion whether and at which accretion rates steady H-burning can continue until the WD approaches M_{Ch}. It

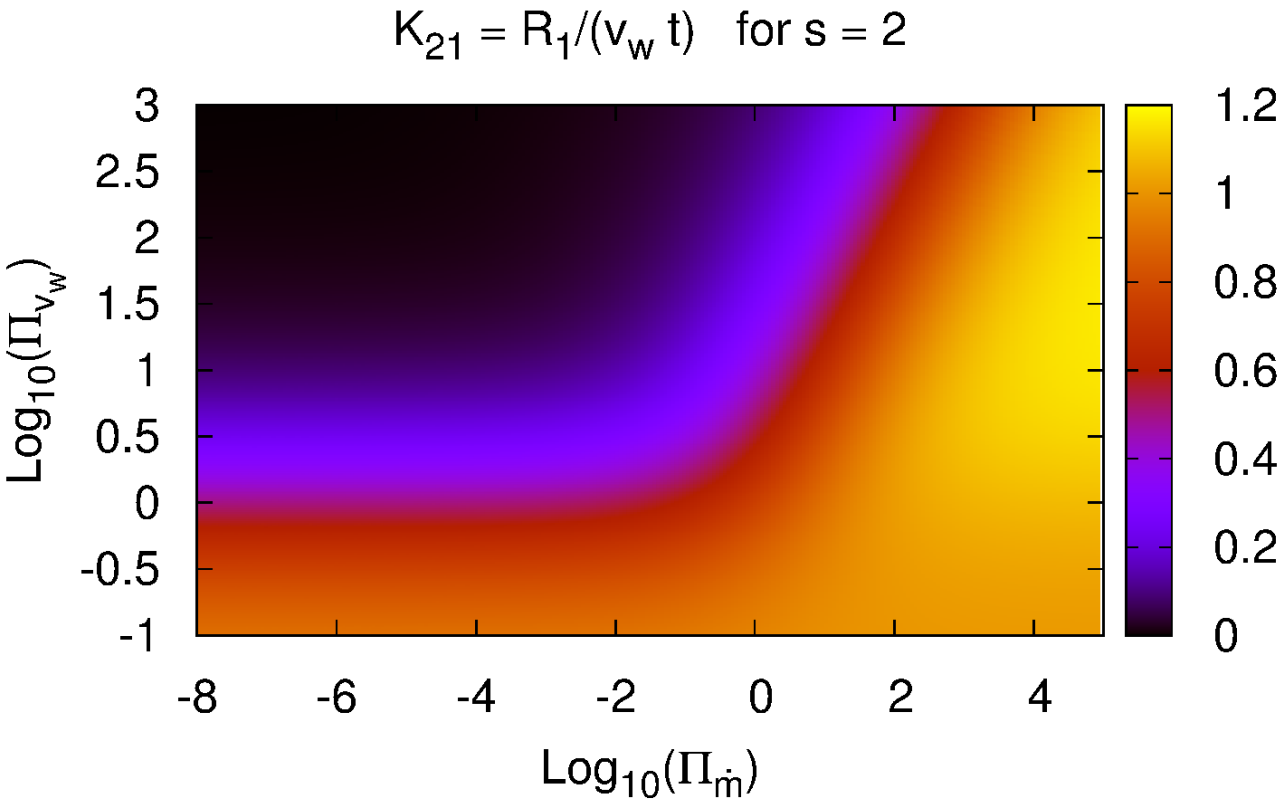

FIG. 8.— Value of K_{21} as a function of v_w and log $K_2(\Pi_{\dot{m}}, \Pi_{v_w})$ where $\Pi_{v_w} = (v_w - v_{w,1})/v_{w,1})$ and $\Pi_{\dot{m}} = (\dot{m}/\dot{m}_1)$. K_{21} is close to constant in the regime of low mass winds running into high mass loss wind, i.e. $log(\Pi_{\dot{m}}) < 0$.

TABLE 2
SAME AS TABLE 1 BUT FOR AN ENVIRONMENT PRODUCED BY A PRIOR WIND (S=2). THE INDEX 1 CORRESPONDS TO THE PRIOR WIND. THE RELATIONS ARE VALID FOR HIGH VELOCITY WINDS RUNNING INTO ENVIRONMENTS PRODUCED BY LOW VELOCITY WINDS (SEE FIG. 7). FOR R_C, R_1, AND u_1, THE RELATIONS ARE VALID FOR $\dot{m}/\dot{m}_1 \lesssim 10^{-4}$. FOR R_2 AND ρ_2, IT IS VALID FOR $\dot{m}/\dot{m}_1 \lesssim 10^{-4}$ AND $v_w/v_{w,1}$ BETWEEN ~ 10 AND 170. τ_m IS CALCULATED BY FORMAL INTEGRAION IN SPICE.

R_C	$\approx$	$v_{w,1}t$
R_1	$\approx$	$v_{w,1}t$
R_2	$\approx$	$1.21\left(\frac{v_{w,1}}{v_w - v_{w,1}}\right)^{1.42} v_w t$
u_1	$\approx$	$\gamma(\gamma+1)^{-1} v_{w,1}$
ρ_2	$\approx$	$0.385\ \dot{m} {v_w}^{-4}\left(\frac{v_{w,1}}{v_w - v_{w,1}}\right)^{-2.84} t^{-2}$
τ_m	$=$	$\dot{m}_1 {v_{w,1}}^{-1} t^{-1} K_{2,\tau}(\Pi_{\dot{m}}, \Pi_{v_w})$

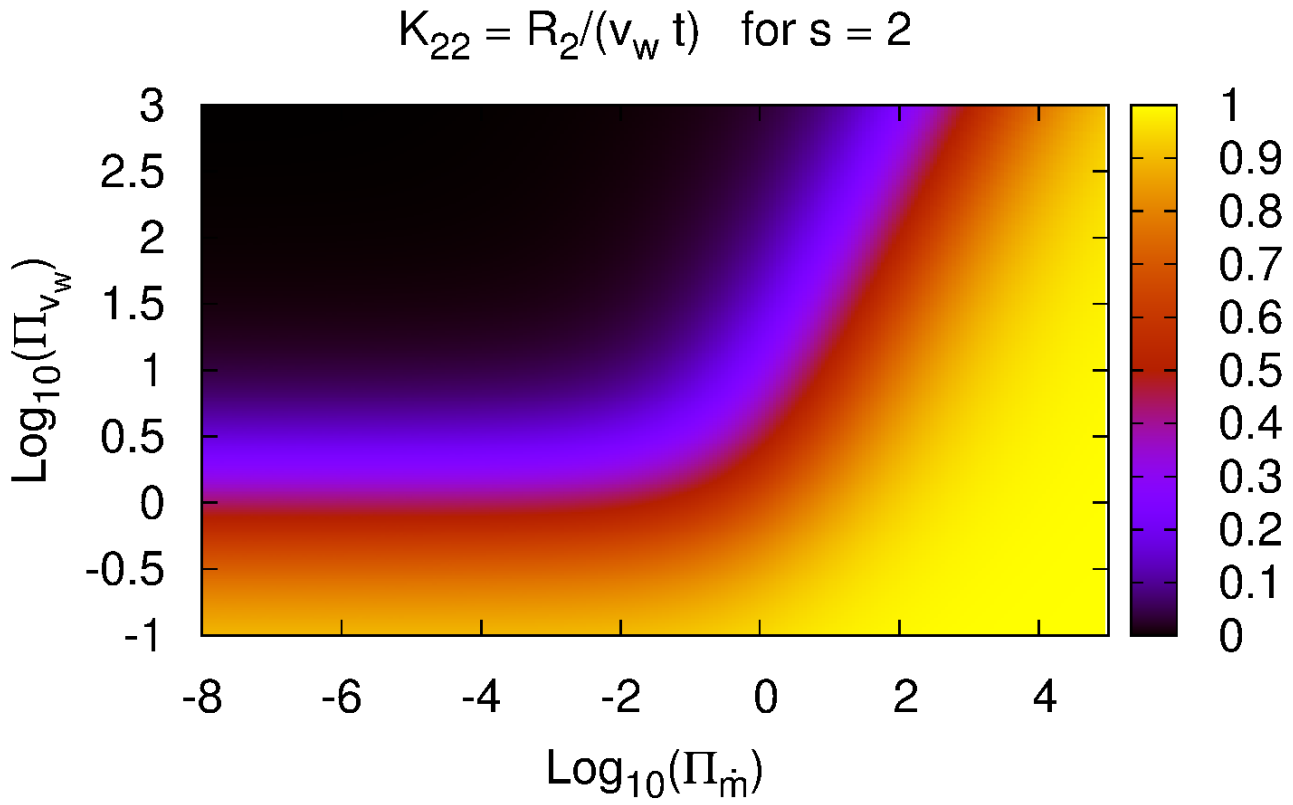

FIG. 9.— Value of K_{22} as a function of v_w and log $K_2(\Pi_{\dot{m}}, \Pi_{v_w})$ where $\Pi_{v_w} = (v_w - v_{w,1})/v_{w,1})$ and $\Pi_{\dot{m}} = (\dot{m}/\dot{m}_1)$. K_{22} is close to constant in the regime of low mass winds running into high mass loss wind, i.e. $log(\Pi_{\dot{m}}) < 0$.

depends on the chemical composition, rotation of the WD, and details of the approximations used (Nomoto 1982b; Starrfield et al. 1985; van den Heuvel et al. 1992; Hachisu et al. 1999; Piersanti et al. 2003a; Yaron et al. 2005; Sako et al. 2008; Hachisu et al. 2012; Bours et al. 2013). For a recent review, see Maoz et al. (2014). In this study, we use the wide range of accretion rates to avoid restricting possible solutions. Thus, we consider time scales t between 10^5 and 4×10^7 years. Larger rates of mass overflow result in over-Eddington luminosity and a strong wind from the progenitor WD with properties typical of RG winds (Hachisu et al. 1996, 2008). Subsequently, we refer to the high-density, low velocity winds as "RG-like". Accretion of He and C/O -rich matter allow much shorter timescales down to the dynamical times of merging WDs.

For accretion disk winds the mass loss rate ranges from 10^{-8} to 10^{-10} solar masses per year; and the wind velocities originating from the disks are believed to be from 2000 to 5000 km/s (Kafka & Honeycutt 2004).

Mass loss in "RG-like" stars are typically between 10^{-6} and 10^{-8} $M_\odot/yr$ with wind velocities between 10 and 60 km/s (Reimers 1977; Judge & Stencel 1991; Ramstedt et al. 2009).

Main sequence star winds are similar to the solar wind (Wood et al. 2002). For solar wind the velocity is between 400 km/s and 750 km/s and the mass loss is $2...3 \times 10^{-14}$ $M_\odot/yr$ (Noci et al. 1997; Feldman et al. 2005; Marsch 2006).

3.1. *Parameterized Study*

In the following, we will assume typical wind parameters as follows: In the "RG-like" case, we use mass loss rates between $\dot{m}$ of 10^{-6}, 10^{-7} and 10^{-8} $M_\odot/yr$, and a wind velocity of 30 km/s. Similar winds can be expected for WDs with high accretion rates. For the case of a MS star donor, we use mass loss rates between 10^{-13}, 10^{-14}, and 10^{-15} $M_\odot/yr$, and $v_w = 500$ km/s. For AD winds the mass loss rate ranges from 10^{-8}, 10^{-9}, and 10^{-10} solar masses per year; a typical rate has been measured to be 10^{-9} $M_\odot/yr$. A wind velocity of 3000 km/s is used. For the duration of the winds, we consider t between 1.5×10^5 and 6×10^8 years with 3×10^5 years for the references.

The outer environment of the system depends on its history including the delay time between the formation of the WD and the onset of the accretion phase. For long delays, we assume an ISM with constant density, i.e. $s = 0$.

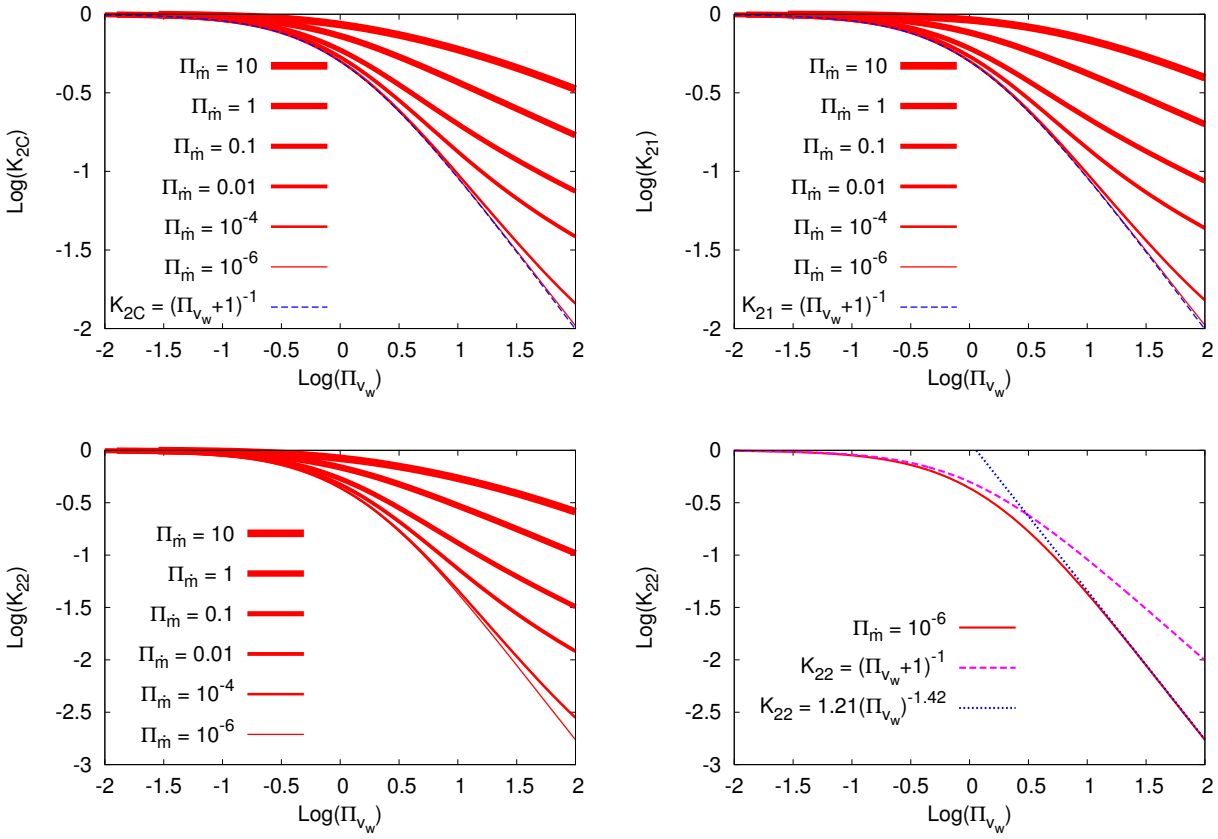

FIG. 10.— $K_{2(C,1,2)}$ as a function of the ratio between inner and outer wind velocity described by $\Pi_{v,w}$ as obtained by cuts at $log(\Pi_{\dot{m}})$ of $10^{-6,-4,-2,-1,0,1}$ indicated by progressively thicker lines. The exact solutions are given in red. We give the solutions for K in comparison to the fits. The approximations are given (magenta and blue, dotted).

For short delay times and small peculiar velocities of the system, the outer environment may be created during the final stage of the progenitor evolution, namely the red giant branch (RGB), horizontal giant branch (HGB) and the asymptotic giant branch (AGB) phase.

3.2. *Results*

3.2.1. *Case I: Constant ISM density*

We first consider scenarios where the wind blows out into a medium of constant density for a wide range of parameters (Tables 3-5). The structures are characterized by I) an undisturbed, inner layer dominated by the stellar wind, II) an inner, shocked region with almost constant, low density and a velocity declining with distance, III) a slowly expanding shell of high density, swept up material, and IV) the ISM. The overall solution is representative for all cases as has been shown in Sect. 2. For the estimate of the equivalent width EW of the Na I doublet at 5890/5896 Å, we use solar abundances, $X_{\rm Na} = 3.34 \times 10^{-5}$. EW is estimated according to Spitzer (1968); Draine (2011). For potassium lines, the corresponding equations apply.

Case Ia: Fast winds from an accretion disk: Table 3 contains calculated results from several cases with different parameters but the same time-scales t. Our reference, model 2 of Table 3, is shown in Fig. 11. It has a mass loss $\dot{m}$ of $10^{-8}\ M_\odot/yr$ and a wind velocity $v_w = 3,000\ km/s$. For the duration of the wind, we choose a duration of 3×10^5 years which, within the SD scenario, corresponds to the evolutionary time for a low mass WD to grow to M_{Ch} at an accretion rate of $\approx 2 \times 10^{-6}\ M_\odot/yr$.

Up to about 2.3 ly, the environment is dominated by the on-going wind. In this region, the particle density drops below 1(100) cm^{-3} at a distance of 0.005(0.0005) ly $\approx 1000(100)\ AU \approx 10^{16(15)}\ cm$ which will be overrun by the SN ejecta within 5(0.5) days. Particle densities below 100 cm^{-3} in this region will hardly affect the light curves or spectra because the swept up mass will be small. Using the same argument, the low densities within 20 ly are too low to affect the hydrodynamics of the SN envelope. A high density, outer shell expands at a velocity of 11 km/s with a velocity dispersion of $\approx 13\% \approx 2\ km/s$. This shell would produce a narrow line Doppler shifted by about 11 km/s. For an interstellar medium, the equivalent width would be about 165 mÅ for the NaID line well comparable to values found by (Phillips et al. 2013) who found between 27 and 441 mÅ in a sample of some 20 SNe Ia.

The morphology of the structures are hardly affected by variations in the wind parameters as expected from the Π

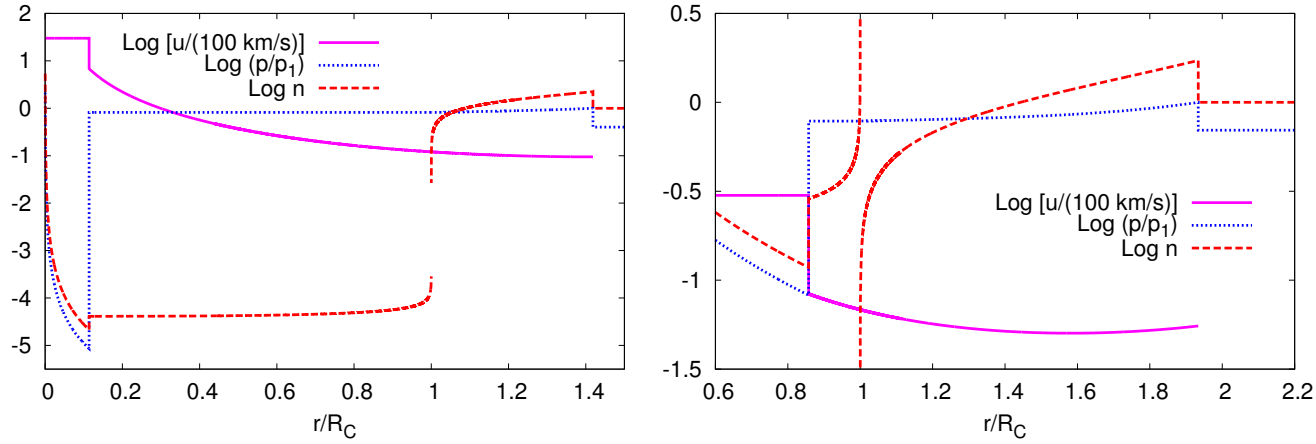

FIG. 11.— Hydrodynamic profile for a wind typical for an accretion disk (left), $v_w = 3000\ km/s$ and mass-loss rate of $10^{-8}\ M_\odot/yr$, and a RG-like wind (right), 30 km/s and mass-loss rate of $10^{-7}\ M_\odot/yr$, running into a constant interstellar medium density of 1 particle per cm^3 after a time of 300,000 years. The contact discontinuity is at 21.7 and 5.45 light-years, respectively. Fluid velocity u (magenta) is normalized to 100 km/s, pressure p (blue) is normalized to the pressure p_1 just inside the outer shock, and particle density n is unnormalized.

TABLE 3
INTERACTION OF WINDS OF AN ACCRETION DISK (AD) WITH A CONSTANT ISM (S=0). NUMERICAL RESULTS ARE GIVEN FOR PARAMETERS TYPICAL FOR THOSE WINDS FOR THE FAP MODEL (SEE TEXT AND TABLE 1). IN ADDITION, WE GIVE THE VELOCITY DISPERSION OF THE SHELL σ_u AND THE OPTICAL DEPTH τ AND EQUIVALENT WIDTH EW OF THE $NaID$ LINE. OUR REFERENCE MODEL IS MARKED BY $*$.

No	n_0 (cm^{-3})	v_w (km/s)	$\dot{m}$ $(M_\odot/yr)$	t (Myr)	t_p (Myr)	R_C (ly)	R_1 (ly)	R_2 (ly)
1	0.1	3000	10^{-8}	0.3	2.36	33.34	41.94	4.89
2*	1.0	3000	10^{-8}	0.3	0.745	20.11	28.53	2.29
3	10.0	3000	10^{-8}	0.3	0.236	11.39	22.02	0.98
4	1.0	3000	10^{-9}	0.3	0.236	11.39	22.02	0.98
5	1.0	3000	10^{-10}	0.3	0.0745	5.80	20.47	0.36
6	1.0	3000	10^{-8}	0.15	0.745	13.70	17.84	1.82
7	1.0	3000	10^{-8}	0.4	0.745	23.44	35.07	2.50

No	u_1 (km/s)	u_c (km/s)	σ_u (km/s)	n_2 (cm^{-3})	τ_m (g/cm^2)	$log(\tau)$	EW_{NaI} $(m\text{Å})$
1	16.56	19.99	0.85	2.07×10^{-5}	2.60×10^{-6}	1.34	157
2*	9.45	12.06	0.62	9.45×10^{-5}	1.91×10^{-5}	2.34	165
3	5.53	6.83	0.32	5.20×10^{-4}	1.71×10^{-4}	3.59	192
4	5.53	6.83	0.32	5.20×10^{-5}	1.71×10^{-5}	2.59	98.4
5	4.50	3.48	0.62	3.94×10^{-5}	1.84×10^{-5}	2.33	163
6	13.34	16.42	0.76	1.50×10^{-4}	1.13×10^{-5}	2.03	180
7	8.16	10.54	0.56	7.95×10^{-5}	2.42×10^{-5}	2.49	157

theorem. However, the actual size of the regions and the densities vary (see Table 3) with dependencies as expected from Table 1. Within the framework of SNe Ia, the ram pressure dominates the ambient pressure which, therefore, hardly affects the solution. Typically, wind from an accretion disk will produce an inner cavity between 5 and 30 ly surrounded by an expanding shell with a velocity of $\approx 5...20\ km/s$. EW (NaID) is ≈ 100 to 200 mÅ. The combination of line shifts and strength allows us to derive the wind parameters.

In our table, we assumed an accretion rate of $\approx 2 \times 10^{-6}\ M_\odot/yr$ which is at the upper limit allowed for stable accretion of hydrogen rich matter. Higher mass loss can be expected for over-Eddington accretion or He or C/O accreting WDs (see Sect. 1). Higher and lower mass loss rates will increase/decrease the size of the cavity but the dependency is relatively weak, $\propto \dot{m}^{1/5}$.

However, the actual size of the region does depend sensitively on the time t of the progenitor evolution as the size of the cavity goes like $\propto t^{3/5}$. In hydrogen accreters, the rate of accretion may be smaller by a factor of 100 and, thus, t may be larger by the same factor which, in turn, will increase the size of the cavity by 16 and decrease shell velocities by about a factor of 6. Shorter durations can be realized if we start with a WD of $1.2M_\odot$, the upper end of mass range for a C/O WD (see Introduction). Indeed, there is some evidence and theoretical arguments that the

TABLE 4
Same as Table 3 but for an "RG-like" wind. Our reference model is marked by ∗.

No	n_0 (cm^{-3})	v_w (km/s)	$\dot{m}$ $(M_\odot/yr)$	t (Myr)	t_p (Myr)	R_C (ly)	R_1 (ly)	R_2 (ly)
8	0.1	30	10^{-7}	0.3	0.0745	5.80	20.47	3.55
9*	1.0	30	10^{-7}	0.3	0.0236	2.75	20.28	1.16
10	1.0	30	10^{-5}	0.3	0.236	11.39	22.02	9.77
11	1.0	30	10^{-6}	0.3	0.0745	5.80	20.47	3.55
12	1.0	30	10^{-8}	0.3	0.0075	1.28	20.27	0.37
13	1.0	30	10^{-7}	0.15	0.0236	2.16	10.17	1.15
14	1.0	30	10^{-7}	2.0	0.0236	5.20	135	1.16
15	0.1	30	10^{-7}	3	0.0745	12.8	203	3.69
16	1.0	30	10^{-7}	3	0.0236	5.96	203	1.17
17	0.1	30	10^{-7}	13	0.0745	20.9	878	3.70
18	1.0	30	10^{-7}	13	0.0236	9.71	878	1.17
19	0.1	30	10^{-7}	50	0.0745	32.8	3377	3.70
20	1.0	30	10^{-7}	50	0.0236	15.2	3382	1.17

No	u_1 (km/s)	u_c (km/s)	σ_u (km/s)	n_2 (cm^{-3})	τ_m (g/cm^2)	$log(\tau)$	EW_{NaI} $(m\text{Å})$
8	4.50	3.48	0.62	4.19×10^{-2}	1.84×10^{-6}	1.33	114
9*	4.37	1.65	0.94	3.75×10^{-1}	1.94×10^{-5}	2.17	231
10	5.53	6.83	0.32	6.62×10^{-1}	1.71×10^{-5}	2.59	98.4
11	4.50	3.48	0.62	4.19×10^{-1}	1.84×10^{-5}	2.33	163
12	4.36	0.77	1.03	3.66×10^{-1}	1.97×10^{-5}	2.14	251
13	4.41	2.60	0.79	3.92×10^{-1}	9.46×10^{-6}	1.94	181
14	4.37	0.47	1.05	3.65×10^{-1}	1.32×10^{-4}	2.96	329
15	4.36	0.77	1.03	3.66×10^{-2}	1.97×10^{-5}	2.14	251
16	4.36	0.36	1.05	3.64×10^{-1}	1.98×10^{-4}	3.13	353
17	4.36	0.29	1.05	3.64×10^{-2}	8.58×10^{-5}	2.77	309
18	4.36	0.13	1.05	3.63×10^{-1}	8.58×10^{-4}	3.77	500
19	4.36	0.12	1.05	3.63×10^{-2}	3.30×10^{-4}	3.35	391
20	4.38	0.05	1.06	3.64×10^{-1}	3.31×10^{-3}	4.35	809

progenitors originate close to the upper end of that mass range (Nomoto et al. 2006; Hoeflich 2006; Sadler 2012) which may reduce the amount of accreted material from ≈ 0.8 to 0.2 $M_\odot$. Thus, the duration of the accretion t may be correspondingly shorter which, in turn, reduces the size of the cocoon and increases the shell velocities by ≈ 2 and 1.5, respectively.

On the other hand, rates for He and C/O accretion can be larger than hydrogen accreters by, at least, the same factor of 100 (Whelan & Iben 1973; Piersanti et al. 2003a; Wang et al. 2009b,a), reducing the size of the shell and increasing the velocity of the shell lines by the same factors. High shell velocities may indicate He- or C/O accreters. Despite the line shifts, systems with high shell velocities can be expected to have smaller low density regions. The SN ejecta have velocities up to about 10 to 20% of the speed of light. For such SNe Ia, we may expect interaction on time scales from 1 to 10 years for our set of parameters.

Case Ib: MS star winds: MS star winds produced by a donor star are expected to show low velocities $v_w = 500$ km/s and a very low mass loss $\dot{m} = 10^{-14}$ $M_\odot/yr$. Although the morphology of the shells remain the same as above, the corresponding regions will be overrun and dominated by wind from the accretion disk. The radius of the reverse shock R_2 show little change for time scales much longer than t_p (see Table 6). As discussed above, R_C becomes unphysical due to mixing in a regime of weak shocks. For SNe Ia, the MS wind component can be neglected.

Case Ic: Slow, RG-like winds may be produced during the RG phase of the donor star or the progenitor prior to the formation of the progenitor WD, or as a result of over-Eddington mass overflow (Table 4). We refer to those as RG-like winds. The resulting structures are very similar to Case Ia but the densities are higher by an order of magnitude (Fig. 11). In particular, the density contrast $n_2/n_0 \approx 0.1$ (see also Table 1). The cocoons are smaller and less pronounced in this case.

For typical properties of the environment, we have to distinguish between winds for an RG donor, RG-like winds from over- Eddington accretion, and the prior RG-phase of the progenitor.

In Table 4, models are shown for RG-like winds for various n_0, $\dot{m}$ and t. As expected, the size of the cavity decreases with n_0 (model 8 vs. 9). We choose t in the range for stable hydrogen accreters (models 8 to 14). As duration t increases, the location of R_2 "stalls" and n_2 is hardly affected because the outer and inner pressure equilibrates $(t/t_p \gg 1)$ as discussed in the Sect. 2.2. See also Table 1. For the same reason, the size of the cavity increases with $\dot{m}$ but n_2/n_0 hardly changes. Typically, RG-like winds will produce an inner cavity between 1 and 10 ly surrounded by an expanding shell with a velocity of ≈ 5 km/s. EW (NaID) is a few hundred mÅ. Note that the scales of RG winds are smaller by an order of magnitude compared to those of AD winds unless those have much lower mass loss than considered in our example above. An RG wind is more likely to form a combined AD-RG wind as discussed below.

TABLE 5
Same as Table 3 but for the combination of an AD- and "RG-like" wind (see text).

No	n_0 (cm^{-3})	v_w (km/s)	$\dot{m}$ $(M_\odot/yr)$	t (Myr)	t_p (Myr)	R_C (ly)	R_1 (ly)	R_2 (ly)
21	1.0	300	1.1×10^{-7}	0.30	0.247	11.68	22.17	3.21
22	1.0	60	1.01×10^{-6}	0.30	0.150	8.85	21.03	4.73
23	1.0	33	1.001×10^{-5}	0.30	0.082	6.15	20.50	3.70

No	u_1 (km/s)	u_c (km/s)	σ_u (km/s)	n_2 (cm^{-3})	τ_m (g/cm^2)	$log(\tau)$	EW_{NaI} $(m\text{Å})$
21	5.62	7.00	0.33	5.33×10^{-3}	1.71×10^{-5}	2.57	100
22	4.88	5.30	0.33	1.17×10^{-1}	1.75×10^{-5}	2.59	100
23	4.52	3.69	0.58	3.49×10^{-1}	1.83×10^{-5}	2.36	154

RG winds from the progenitor prior to the WD phase (models 15-20) will produce a similar structure as an RG donor in a system with high accretion rates ($\sim 10^{-6}\ M_\odot/yr$) but are systematically larger because the longer duration t. This wind may form an environment for subsequent winds. Progenitor system winds may run into this environment if the delay time between the formation of the WD and the onset of the accretion is sufficiently short, and if the peculiar velocity of the system is small. The peculiar velocities of stars show a wide range with a typical value of 25-50 km/s for the Galactic plane ((Griv et al. 2009), and references therein). Here, the duration of the wind is given by the evolutionary time scale of the RG phase rather than the time to reach M_{Ch}. For models 15-18, we use t corresponding to the post-main sequence life time of 5 and 8 $M_\odot$ stars with a mass loss rates of $10^{-7}\ M_\odot$ The resulting total mass loss is 1.3 and 0.3 $M_\odot$ for the 5 and 8 $M_\odot$ star, respectively (Schaller et al. 1992; Chieffi et al. 2001).

The environment formed by a wind consists of inner region with $s \approx 2$ with a size R_2 and a low density void ($s \approx 0$) of size R_C. The resulting size of the void, R_C, is typically 10-20 ly. The duration t can be increased by lower main sequence masses for the progenitor. However, then, the amount of mass lossed prior of forming a WD of $M(WD) \approx 0.6\ M_\odot$. Using a mass loss of $10^{-7}\ M_\odot$ and $v_w = 30\ km/s$, the maxima in R_C and R_2 is produced by a 3.6 $M_\odot$ star: $\approx 33\ ly$ and $\approx 3.7\ ly$, respectively (models 19, 20, Table 4). Models with durations of 3, 13 and 50 Myr correspond to progenitor stars of 8, 5, and 3.6 $M_\odot$.

We note that long durations may also be produced during the evolution of the progenitor system if the hydrogen accretion rate is close to the lower limit of $\sim 10^{-8}\ M_\odot/yr$, though this low a rate may not allow for stable accretion for WD close to M_{Ch} (Piersanti et al. 2003b). Models with RG-like winds may correspond to systems with over-Eddington accretion and a MS donor star (models 15-20). For those long duration RG-like winds, the resulting cavities can be ≈ 15 to 33 ly and high EW of $\approx 500\ m$Å.

Case Id: Fast wind from an accretion disk combined with mass loss from RG donor star or super-Eddington accretion: If we have a system with both a dense RG donor wind and an accretion disk wind, the two will combine. The inner interaction region will be RT unstable and mix fast (Fig. 12). They can be expected to form a uniform wind with an acceleration region. Assuming momentum conservation and our reference models for the AD wind and "RG-like" winds, we obtain a total mass loss rate of $\approx 10^{-5,-6,-7}\ M_\odot$ and wind velocity of $\approx 33, 60$ and 300 km/s (see models 21-23, Table 5).

This case applies in system with high peculiar velocity. There, the system has moved out of the environment formed during the stellar evolution of the progenitor. The cavities are somewhat larger by about a factor of 2 compared to the RG-like wind cavities, surrounded by an expanding shell of a similar velocity and EW (NaID). The larger cavity will result in a slower evolution of the narrow lines.

Extremely low Density Environments: In case of long delay times of SNe Ia, the progenitor system may have wandered away from the galactic disk into the halo, in a regime of very low densities Graham et al. (2015a), or in a hot-ISM Fesen et al. (2007), or in the constant density region II of the cavity from prior mass loss. In Table 7, some examples are given for constant density with particle densities between 10^{-2} to $10^{-3}\ cm^{-3}$. Most likely, the donor star will not be a RG star. The inner, low density region is expected to be of the order of or larger than $50 - 100\ ly$. EW(NaID) are between 20 to 100 mÅ and show increased Doppler shifts of ≈ 30 to 50 km/s or larger for even lower density than found in the vicinity of SN1885 Fesen et al. (2007). In conclusion, of all of wind components analyzed separately, the AD wind component will dominate the formation of cocoons.

3.2.2. *Case II: Environments produced by Winds*

Now we consider the scenario where the wind of the progenitor system runs into a nearby environment produced by a prior mass loss ($s = 2$). "Nearby" means that the reverse shock R_2 produced by the prior mass loss must be larger than the size of the region produced by the wind of the system. Otherwise the interaction region will move into a region of constant density, shocked RG wind, or the ISM. Moreover, the speed of the ongoing wind must exceed that of the outer wind. For our discussion, we disregard the effect of prior mass loss by a MS wind because it produces on an cocoon of $< 0.005\ ly$ Table 6 and consider parameters only in which the prior wind can be produced by an RG star.

Case IIa: Fast wind from an accretion disk and a non-RG donor star: If the donor star is a compact

TABLE 6
SAME AS TABLE 3 BUT FOR A MS WIND, INCLUDING THE AMBIENT PRESSURE (FAP MODELS). OUR REFERENCE MODEL IS MARKED BY ∗. VALUES ARE GIVEN FOR THE RADIUS OF THE CONTACT DISCONTINUITY AND THE INNER SHOCK USING PARAMETERS TYPICAL FOR THE WIND OF A MAIN SEQUENCE STAR, AND USING THE SOLUTION INCLUDING THE AMBIENT PRESSURE (FAP MODELS). FOR TIMES (T) MUCH LARGER THAN t_p, THE LOCATION OF THE REVERSED SHOCK BECOMES STATIONARY AND CLOSE TO THE DISTANCE $R_{2,\mathrm{PE}}$ EXPECTED FROM EQUILIBRATING THE PRESSURE AT THE REVERSED SHOCK WITH THE AMBIENT MEDIUM. IN ADDITION, MODELS WITHOUT OUTER PRESSURE ARE GIVEN AND MARKED BY "REM.". THIS SHOWS THE IMPORTANCE OF THE PRESSURE TERM FOR $t/t_p \gg 1$ IN THE EXTREME CASE. HOWEVER, FOR WINDS RELEVANT IN SNE, THE DIFFERENCE IS OF THE ORDER OF SEVERAL % (SEE TEXT, AND FIG. 2).

No	n_0 (cm^{-3})	v_w (km/s)	$\dot{m}$ $(M_\odot/yr)$	t (Myr)	t_p (yr)	R_C (ly)	R_2 (ly)	$R_{2,\mathrm{PE}}$ (ly)
1	0.1	500	10^{-14}	40	393	0.921	0.00477	0.00390
Rem.	"	"	"	"	-	20.0	0.481	
2*	1	500	10^{-14}	40	124	0.427	0.00151	0.00123
Rem.	"	"	"	"	-	12.6	0.241	
3	10	500	10^{-14}	40	39.3	0.198	0.000477	0.000390
Rem.	"	"	"	"	-	7.94	0.121	
4	1	500	10^{-13}	40	393	0.921	0.00477	0.00390
5	1	500	10^{-15}	40	3.93	0.198	0.000477	0.00039
6	1	500	10^{-14}	2	124	0.157	0.00151	0.00123
7	1	500	10^{-14}	600	124	1.05	0.00151	0.00123
8	0.1	500	10^{-14}	0.3	393	0.180	0.00477	0.00390
9	1	500	10^{-14}	0.3	124	0.0836	0.00151	0.00123
10	10	500	10^{-14}	0.3	3.93	0.0388	0.000477	0.000390
11	1	500	10^{-15}	0.3	3.93	0.0388	0.000477	0.000390
12	1	500	10^{-14}	0.4	124	0.0921	0.00151	0.00123

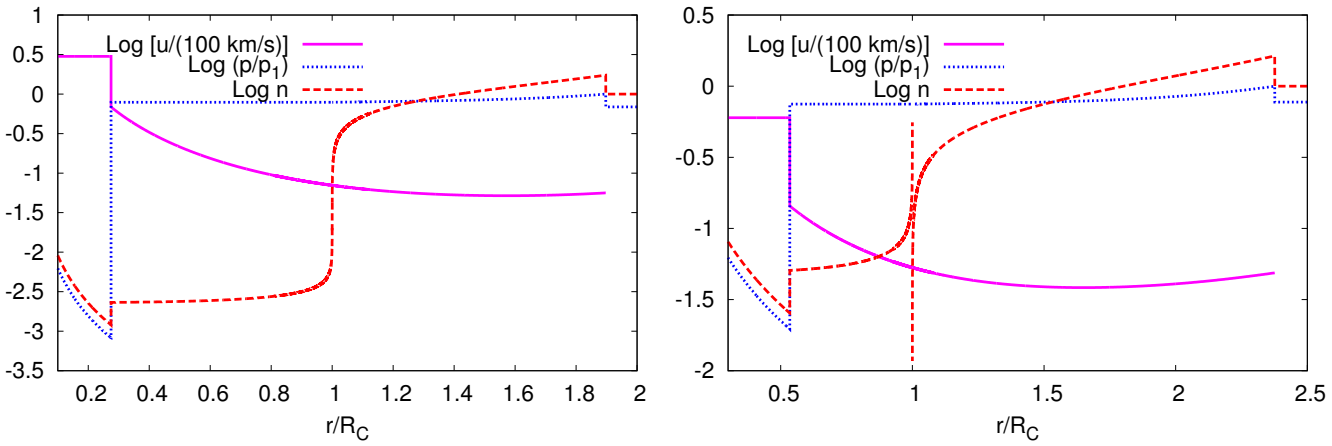

FIG. 12.— Same as Fig. 11 but for a mixture of AD plus RG-like winds. Left and right are shown models no. 21 and 22 from Table 5, respectively.

object like a MS or He-star, the AD wind will dominate. Examples are shown in Table 8. As reference, some typical parameters are $\dot{m}_1 = 10^{-6}\ M_\odot/yr$, $v_{w,1} = 30\ km/s$, $\dot{m} = 10^{-10}\ M_\odot/yr$, $v_w = 3000\ km/s$ and a total run time of 1.5×10^5 years. Again, we can identify the different zones as above (Fig. 13). The density contrast between the inner bubble within R_C is smaller than in the constant density case, i.e. a factor of 10^{-2}, but the density at R_C is significantly lower than the ISM. This results in an an "ultra-low" density bubble of $n \approx 4 \times 10^{-8}\ cm^{-3}$.

Moreover, this solution shows a qualitative different feature compared to the constant density ISM: We see a very thin and dense shell with particle densities $\leq 10^2\ cm^{-3}$ and a thickness of light-weeks to light-months (Fig. 13). The resulting shell produces a narrow, optically thick NaID line with small equivalent width EW of 0.24 mÅ, Doppler shifted by about $u_c = 240\ km/s$ and a width of $\approx 23\ km/s$. We note that, to first order, EW $\propto \dot{m}$ (model 1, Table 8).

Case IIb: Fast wind from an accretion disk combines with a "RG-like" wind: If we have a system with a dense RG donor and wind plus an accretion disk wind, they would form a uniform wind with an acceleration region (Fig. 14). We use the same parameters as in Sect. 3.2.1 but omit the mixed wind with the highest mass loss because it's velocity will be comparable to the wind velocity of the surrounding medium. As expected, the cavities are smaller than the AD-wind case, and EW(NaID) and its Doppler shift are larger.

Comparing interaction regions of environments created by winds with constant density ISM, the typical scales are larger in the former and the resulting narrow lines show a larger blue-shift with smaller EW.

TABLE 7
Same as tables 3 and 6 but for very low density ISM typical for the galactic halo and elliptical galaxies.

No	n_0 (cm^{-3})	v_w (km/s)	$\dot{m}$ $(M_\odot/yr)$	t (Myr)	t_p (Myr)	R_C (ly)	R_1 (ly)	R_2 (ly)
1	0.01	3000	10^{-8}	0.4	2.36	63.8	77.2	11.21
2	0.001	3000	10^{-8}	0.4	23.6	102	121	22.7
3	0.01	30	10^{-7}	50	0.236	70.8	3368	11.7
4	0.001	30	10^{-7}	50	0.745	152	3377	36.9

No	u_1 (km/s)	u_c (km/s)	σ_u (km/s)	n_2 (cm^{-3})	τ_m (g/cm^2)	$log(\tau)$	EW_{NaI} $(m\text{Å})$
1	24.36	28.67	1.08	1.72×10^{-6}	4.67×10^{-7}	0.49	104
2	39.6	45.87	1.58	4.21×10^{-7}	7.18×10^{-8}	-0.48	24.0
3	4.32	0.25	1.05	3.62×10^{-3}	3.29×10^{-5}	2.35	272
4	4.36	0.55	1.04	3.65×10^{-4}	3.29×10^{-6}	1.36	193

TABLE 8
Interaction of winds with an environment produced by RG wind originating from the progenitor WD ($v_{w,1} = 30\ km/s$, $s = 2$). The index 1 corresponds to the prior mass loss. Models 1-7 and 8-9 show the results for an AD-wind and a combination of a AD and "RG-like" wind, respectively (Tables 3 & 5).

No	$v_{w,1}$ (km/s)	$\dot{m}_1$ $(M_\odot/yr)$	v_w (km/s)	$\dot{m}$ $(M_\odot/yr)$	t (Myr)	R_C (ly)	R_1 (ly)	R_2 (ly)
AD								
1	30	10^{-6}	3000	10^{-9}	0.3	67.7	74.2	16.4
2	30	10^{-7}	3000	10^{-9}	0.3	122	138	39.3
3	30	10^{-8}	3000	10^{-9}	0.3	240	278	106
4*	30	10^{-7}	3000	10^{-8}	0.3	240	278	106
5	30	10^{-7}	3000	10^{-10}	0.3	67.7	74.2	16.4
6	30	10^{-7}	3000	10^{-9}	0.15	60.8	69.1	19.6
7	30	10^{-7}	3000	10^{-9}	0.4	162	184	52.4
AD+RG-like								
8	30	10^{-7}	300	1.1×10^{-7}	0.3	114	129	91.8
9	30	10^{-7}	60	1.01×10^{-6}	0.3	51.3	54.9	50.0

No	u_c (km/s)	n_2 (cm^{-3})	τ_m (g/cm^2)	$log(\tau)$	EW_{NaI} $(m\text{Å})$
AD					
1	67.7	1.7×10^{-7}	1.59×10^{-8}	-2.02	5.63
2	122	2.9×10^{-8}	1.18×10^{-9}	-3.34	0.420
3	239	4.0×10^{-9}	6.96×10^{-11}	-4.80	0.0248
4*	239	4.0×10^{-8}	6.96×10^{-10}	-3.80	0.248
5	67.7	1.7×10^{-8}	1.59×10^{-9}	-3.02	0.566
6	122	1.2×10^{-7}	2.36×10^{-9}	-3.02	0.837
7	122	1.6×10^{-8}	8.86×10^{-10}	-3.45	0.315
AD+RG-like					
8	114	5.9×10^{-6}	1.59×10^{-9}	-2.92	0.565
9	51.3	9.1×10^{-4}	5.05×10^{-9}	-1.86	1.79

3.3. *Application to SN 2014J*

We will now explore the application of our semi-analytic models to the case of SN 2014J.

Background: This object was discovered in January of 2014 in a high density region of the nearby M82. The higher than average ISM densities and the small proximity of the host make SN 2014J an excellent candidate for investigating the interaction of the SN with the environment. This gives us a premier opportunity to implement our models and make predictions.

Observational constraints for the environment and progenitor are obtained from searches for X-rays (Margutti et al. 2014), time-dependence of high-resolution spectra of narrow potassium lines formed in the environment(Graham et al. 2015b), IR imaging (Kelly et al. 2014), and radio (Pérez-Torres et al. 2014). X-rays and radio provided the most stringent constraints on the average density of ions in the environment. In the case of SN 2014J, X-rays and radio luminosities at maximium light probe the wind from the progenitor system (region I in Fig. 1).

When the SN material propagates into the circumstellar surrounding, a shock is formed and leads to the acceleration

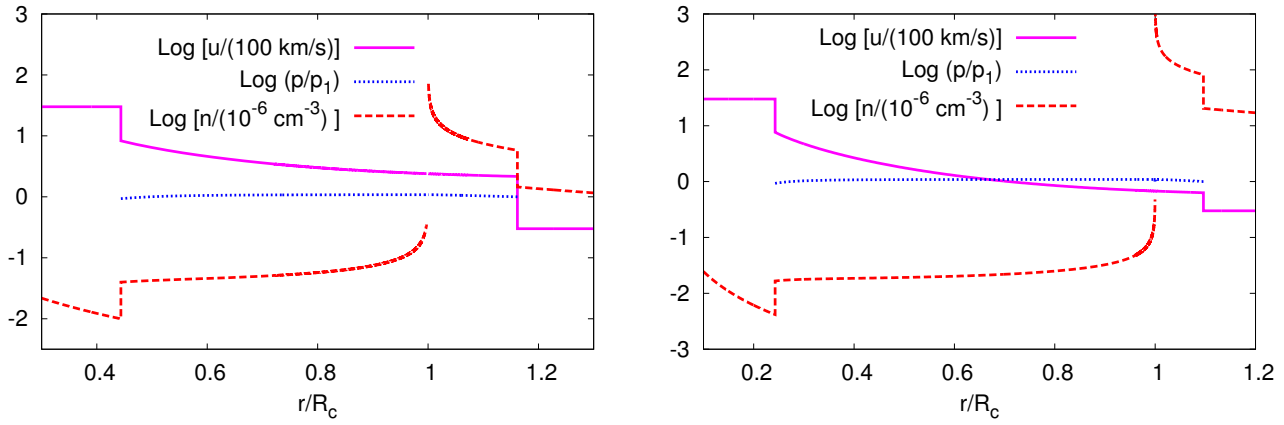

FIG. 13.— Hydrodynamic profile for a wind typical of an accretion disk running into an r^{-2} density profile of prior mass loss. In the left figure, a wind of velocity $v_w = 3000\ km/s$ and mass-loss rate of $\dot{m} = 10^{-8}\ M_\odot/yr$ runs into another wind of mass loss $\dot{m}_1 = 10^{-7}\ M_\odot/yr$ and $v_{w,1} = 30\ km/s$ for a time of 300,000 years. The right figure is the same except the ongoing mass loss rate $\dot{m} = 10^{-10}\ M_\odot/yr$. The contact discontinuity is at 240 and 67.7 light years, respectively. Fluid velocity u (magenta) is normalized to 100 km/s, pressure p (blue) is normalized to the pressure p_1 just inside the outer shock, and particle density n is normalized to $10^{-6}\ cm^{-3}$. Note that the particle density normalization used is much smaller than in the constant density case.

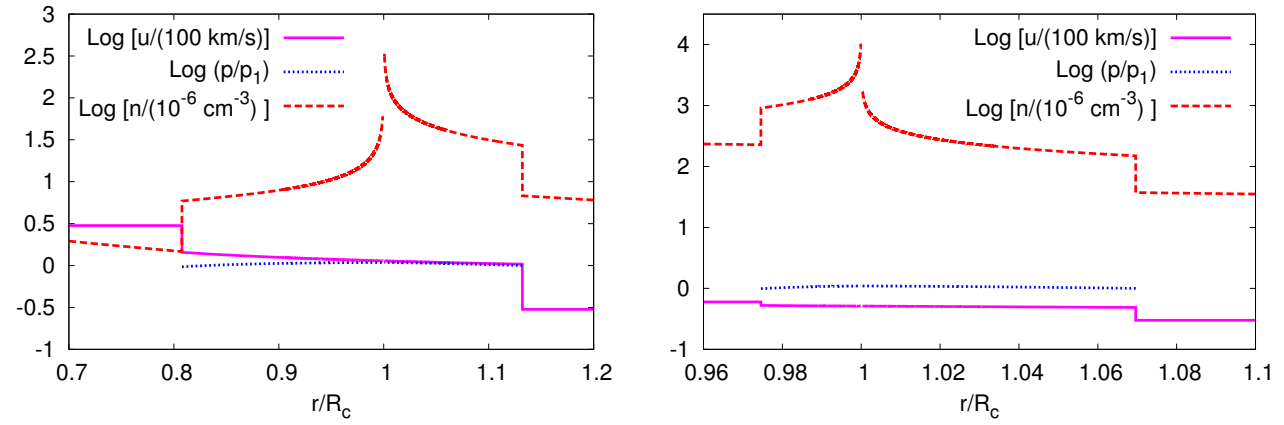

FIG. 14.— Same as Fig. 13 but for a mixture of AD plus RG-like winds. Left and right are shown models 8 and 9 from Table 8, respectively.

of partially or fully relativistic electrons with a power-law distribution $n_e(\gamma) = n_0\gamma^{-p}$ with p between 2 and 3, which produce X-ray and radio emission. From radio observations of SNe Ib/c, Chevalier & Fransson (2006) find $p \approx 3$. Because the outer layers of a SNe Ia and SN Ibc have similar structure, abundances and velocities, we use this value in the following.
For X-rays (Margutti et al. 2012a), L_ν is given by

$$L_\nu = 16500\,\epsilon_e^2 \left(\frac{\dot{m}/v_w}{M_\odot\,yr^{-1}\,km^{-1}\,s}\right)^{0.64} \left(\frac{t}{d}\right)^{-1.36} \nu^{-1} \left(\frac{L_{\rm bol}}{erg\,s^{-1}}\right) \frac{erg}{s\,Hz}. \quad (51)$$

For the radio (Pérez-Torres et al. 2014), L_ν is given by

$$L_\nu = 5.81\times10^{-9}\,\epsilon_{\rm e}^{1.71}\,\epsilon_{\rm B}^{1.07} \left(\frac{\dot{m}/v_w}{M_\odot\,yr^{-1}\,km^{-1}\,s}\right)^{1.37} \left(\frac{t}{d}\right)^{-1.55} T_{\rm bright}\ \nu^{-1}\frac{erg}{s\,Hz}. \quad (52)$$

The parameters are the fraction of relativistic electrons $\epsilon_{\rm e}$, the energy fraction in the magnetic field $\epsilon_{\rm B}$, and the brightness temperature $T_{\rm bright}$ which, based on observations, can be expected to be $\approx 10^{11}K$ (Readhead 1994). Margutti et al. (2014) and Pérez-Torres et al. (2014) use a value of 0.1 for $\epsilon_{\rm e}$ and $\epsilon_{\rm B}$.

If the supernova shell runs into a constant density environment, the X-ray luminosity is given by

$$L_\nu = 6.44\times10^{-5}\,\epsilon_e^2 \left(\frac{n_0}{cm^{-3}}\right)^{0.5} \left(\frac{t}{d}\right)^{-0.45} \nu^{-1} \left(\frac{L_{\rm bol}}{erg\,s^{-1}}\right) \frac{erg}{s\,Hz}. \quad (53)$$

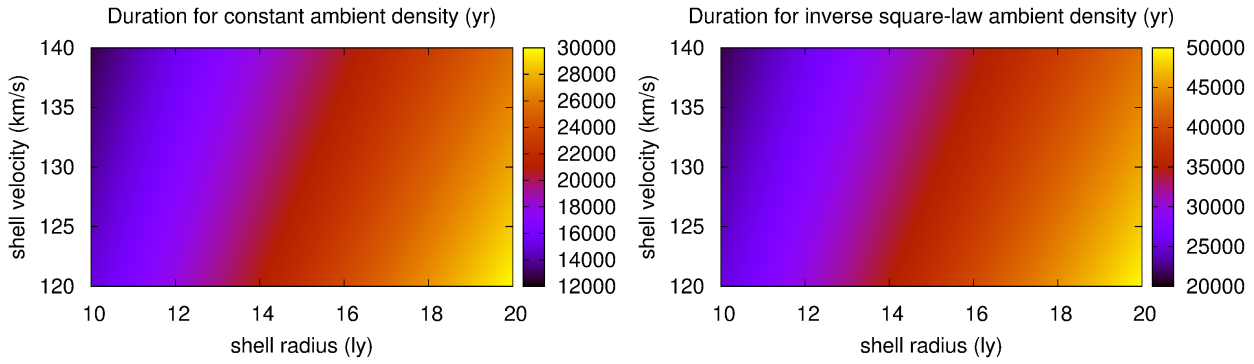

FIG. 15.— Allowed duration of the wind for SN 2014J as a function of R_c and $\dot{R}_c$, for constant density environment, s=0 (left), and wind environment, $s = 2$ (right).

For late times when the SN shock runs into region II (Fig. 1), the radio luminosity is given by

$$L_\nu \propto T_{\rm bright}\, \epsilon_{\rm e}^{0.86}\, \epsilon_{\rm B}^{1.07}\, n_{\rm ISM}^{1.27}\, t^{0.88}. \tag{54}$$

We note that region II has a constant density. Thus, we expect the radio luminosity to increase with time. Densities in our models of region II (see Fig. 1) are two to four orders of magnitude smaller than limits discussed above. However, radio must be expected when the SN shockfront hits the shell after 10 to 100 years after the explosion.

In the case of SN 2014J running into a constant density medium and from radio observations, Pérez-Torres et al. (2014) found an upper limit $n_0 \lesssim 1.3$ particles per cm^3. The same luminosity can be produced in a wind with $\dot{m} \lesssim 7.0 \times 10^{-10} \times v_w/(100\ km/s)\ M_\odot/yr$. The neutral lines and the IR emission indicate shells at distances between 10 and 20 ly expanding at velocities between $120 - 140\ km/s$. Margutti et al. (2014) and Pérez-Torres et al. (2014) concluded from their X-ray and radio observations that a DD system was the likely progenitor. However the findings of (Graham et al. 2015b,b) led them to favor a SD progenitor, although excluding a Red Giant as donor.

In light of the different conclusions, we will apply our analytic description to explore the wide range of parameters within the observational limits from the radio- and X-rays. For the outer environment, we consider both an interstellar medium with constant density, s=0, and one consisting of a wind, s=2, produced during the stellar evolution history.

The X-ray and radio observations provide limits on the far-inside region (region I) within the contact discontinuity (Figs. 11 and 13). In order to apply this constraint to our parameter space we will consider our three cases: RG-like wind, MS star wind, and wind originating from the accretion disk. Case I: If the environment is produced by an ongoing RG-like wind with a velocity of 30 km/s, the mass loss would have to be $\dot{m} \lesssim 2.1 \times 10^{-10}\ M_\odot/yr$ which is much too low for RG wind. Ongoing RG-like wind from the donor star is also very unlikely to be consistent with the IR imaging (Kelly et al. 2014). If the environment is formed by a RG-like wind, it must originate from the progenitor star prior to the formation of the WD. Case II: If the wind originates from a MS star with 500 km/s, radio limits would allow $\dot{m} \lesssim 3.5 \times 10^{-9}\ M_\odot/yr$. Case III: For an AD wind with 3000 km/s, this means $\dot{m} \lesssim 2.1 \times 10^{-8}\ M_\odot/yr$, well within limits discussed in the introduction.

Narrow circumstellar lines have also been used to probe the environment close to the contact discontinuity (e.g. Fig. 1). Using ionization models, Graham et al. (2015b) attributed the blueshifted K I and NaI D absorption features to circumstellar shells at $\sim 10 - 20\ ly$ at velocities of $\sim 120 - 140\ km/s$. A further reduction of the parameter space comes from the limits on X-rays and radio. Using our models, we can infer what kind of progenitor wind (and system) could have produced such shells expanding at the proper velocity and distance with the duration of the wind as a free parameter.

Analysis of SN 2014J: In the following, we want to apply our analysis by combining the tools of the last section with the observations of SN 2014J. For finding allowed parameters, we use the given distance and velocity of the shells in combination with wind parameters for the AD-, MS-, RG-like and "RG-like plus AD" winds.

1.) As a first step, we want to determine the allowed duration of the wind t using the shell velocities and distance as given by (Graham et al. 2015b). Assuming the shells are at $R_{\rm C}$ and the expansion velocity at $\dot{R}_{\rm C}$, we can use equation 8 to estimate the allowed range for the duration of the wind (Fig. 15).

2.) In a second step, we make use of the Π-theorem to determine combinations of n_0, $\dot{m}$ and v_w. Because the solutions depend on one and two Π groups for constant ISM and wind-environments, respectively, we have to consider two cases.

Case I: For the constant density environment (s=0), the solutions can be described in the Π space by a unique parameter $\mu = \frac{\dot{m} v_w^2}{n_0}$. We we have to find μ from the observations and step one as described above (Fig. 16). Assuming a particle density of the ISM between 0.1 and 10 cm^{-3}, the allowed range for $s = 0$ in the $\dot{M}$-v_w-space is shown in Fig. 17. Note that the allowed range has linear boundaries because the exponential dependence of the free parameter

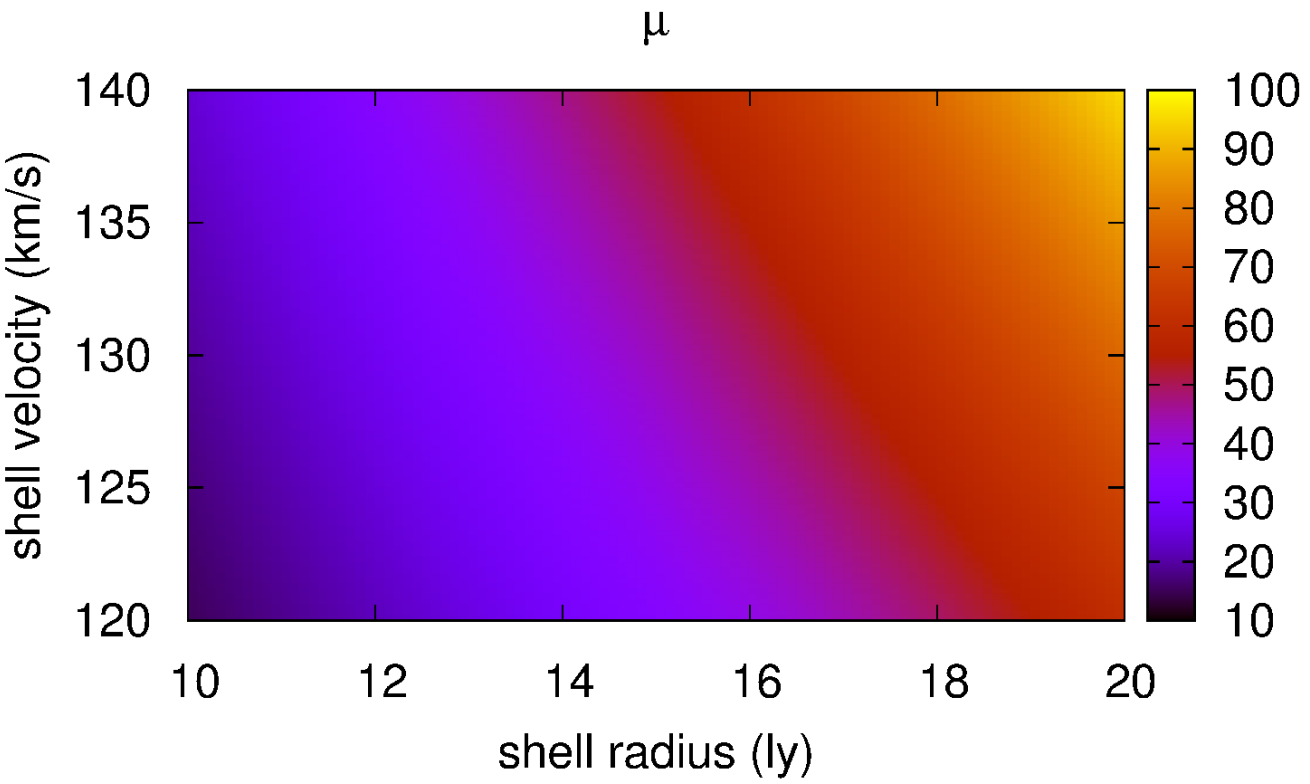

FIG. 16.— Determination of $\mu = \dot{m}{v_w}^2/n_0$ by observations. μ is given as a function of the velocity of the shell and the shell radius in the range given by (Graham et al. 2015b). We assume particle densities of the ISM between 0.1 and 10 cm^{-3}. We find a range of possible solutions $\mu(SN2014J)$ between 15.11 and 95.85 in units of $(M_\odot/yr)(km^2/s^2) \div (cm^{-3})$. Here, the range of μ is given by the extrema in shell velocity and radius.

(see Table 2). The minimum and maximum of μ are found by the values in the lower left and upper right of Fig. 16, respectively. In Fig. 17, the allowed range of μ in the $\dot{m} - v_w$ space is shown in bright green. A constant density may also be produced in region II of prior winds (Fig. 1).

Case II: For ISM environments produced by a wind (s=2, region I), the allowed solutions depend on two Π groups, $\Pi_{\dot{m}}$ and Π_{v_w} (eq. 27 and 28) which relate the mass loss rates and velocities of the interacting winds. Possible solutions are linear in time (eq. 8). Thus, $K_{2C} = R_C/(v_w t) = \dot{R}_C/v_w$. Possible solutions depend only on the shell velocity which can be measured directly from the spectra Graham et al. (2015b). Note that the velocity $\dot{R}_C$ equals the matter velocity. Because it varies slowly in this region (see Fig. 13), the Doppler shift of lines is a good measure of $\dot{R}_C$. Knowing v_w, the original wind velocity is given for any Π_{v_w}. $\Pi_{\dot{m}}$ gives the ratio between the ongoing and the outer wind mass loss rates. We assume that the progenitor wind has the parameters given by a RG star as discussed in Sect. 3. To solve for the implicit condition imposed given by the observations and possible model solutions, a standard rejection technique is applied. We use a Monte Carlo Scheme to sample the parameter space of the ongoing wind for acceptable solutions for $v_{w,1}$. For a given wind parameter of the outer wind, we test each position in Fig. 7 (or the lookup table) for whether the resulting wind velocity $v_{w,1}$ is consistent with an RG wind. If it is, we accept the possible solution. The lines of solutions found in this manner are shown in Fig. 17. The line widths are given by the range of RG wind properties accepted to be consistent with a solution.

3.) In a third step, finally, we compare the allowed range in parameter space with the ranges consistent with our three cases. The ranges of $\dot{m}$ and v_w for each type of wind is presented as a box.

A comparison between the predicted ranges for various winds and the allowed range for SN 2014J constrains the possible progenitor properties. In addition, we marked the parameter range excluded from the lack of X-ray and radio detections. The possible wind parameters for SN 2014J and the location of typical RG, MS and AD winds are shown in Fig. 17. In the figure, we use the quantity $\delta \equiv log_{10}(\dot{m}/v_w)$ as an abbreviation. In addition, we show the allowed region for an environment produced by an RG wind of the progenitor prior to the WD formation.

For constant ISM environments (Case I), there is obviously no overlap between regions allowed from the observations

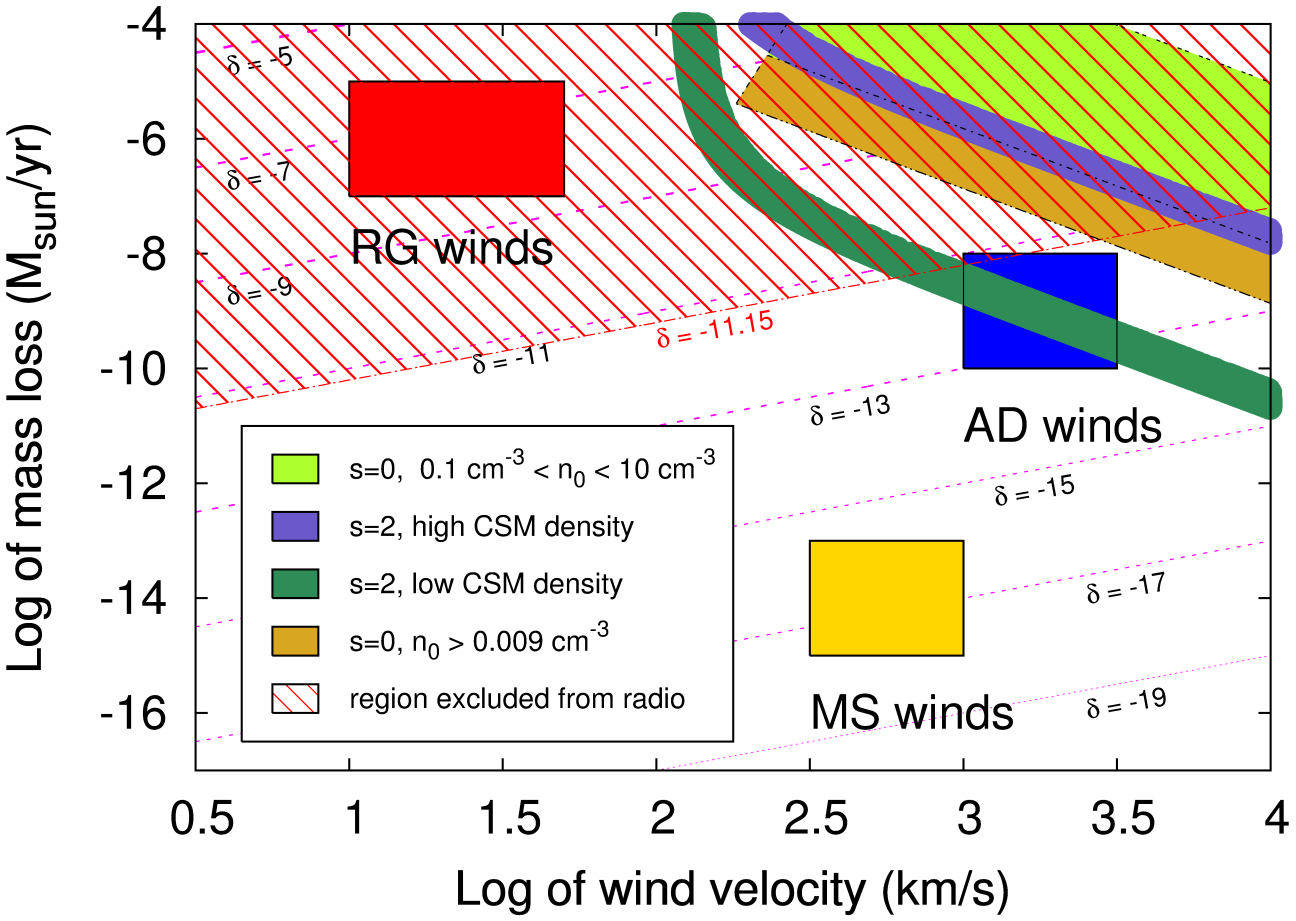

FIG. 17.— Parameters for SN 2014J in the $\dot{m}$-v_w-space as constrained from the spectra and the X-ray and radio luminosities. We give the lines of constant luminosities L_ν for $\delta := log_{10}(\dot{m}/v_w)$ which can be obtained by eqs. 51 and 52. The red, striped area is the forbidden region based on radio and X-ray observations of SN 2014J ($\delta \gtrsim -11.15$). Note that the radio limit from 2011fe gives $\delta \gtrsim -11.22$ (Chomiuk et al. 2012b). The bright green area indicates the allowed range for SN 2014J for constant density environments with particles densities between 0.1 and 10 cm^{-3}. A RG wind prior to the formation of the WD may produce a r^{-2} power law (region I) and a pre-existing constant density surrounding (region II) as low as 0.009 cm^{-3} (see Sect. 3.3 and Fig. 1). The thick, curved lines correspond progenitor winds running into region I of a prior RG wind with $(\dot{m}/v_w)$ in $(M_\odot/yr)/(km/s)$ of $(10^{-7}/60)$ and $(10^{-5}/20)$ which produce low and high CSM, respectively. These lines bracket the range of possible prior RG winds. Their widths indicate the range of solutions of possible AD or RG-like progenitor winds (see text). The boxes indicate the range observed of ongoing RG, MS and AD winds as discussed in Chapter 3. Note that the variations in wind properties are not well known.

and the parameter space of solutions. Constant particle density environments ranging from 0.1 to 10 cm^{-3} can be ruled out. However, a very low density ISM of $\lesssim 0.01$ cm^{-3} is consistent.

We find two other possible solutions both of which require an environment formed by a prior RG-phase of the progenitor (Case II). In either case, we will need a short delay time between the formation of the WD and the explosion.

As discussed above, a wind from the progenitor prior to the WD phase will produce an inner structure with a density close to $\propto r^{-2}$ (region I, Fig. 1), and an outer cocoon of constant, low density (s=0, region II) which is lower than the ISM by about an order of magnitude. The lower limit for the particle density in region II is ≈ 0.009 cm^{-3} which widens the regime of solutions for s=0.

The AD wind may either interact in the r^{-2} or constant density region. In either case, we can exclude RG or RG-like winds from the progenitor system. A RG star as the donor star can be ruled out, too, by the X-rays and radio. This finding is also consistent with the lack of a RG remnant at the location of SN 2014J.

Within the scenario of M_{Ch} explosions, AD winds are consistent with both interaction in region I and II. AD winds are also supported by the high Doppler shifts of the narrow lines reported by (Kelly et al. 2014).

For further constraints, we want to discuss the formation of the necessary wind environment formed from prior mass loss which created the RG-cocoon to, at least, 10 to 20 ly. As discussed above, we use $v_w = 20$ to 60 km/s, mass loss rates between 10^{-5} and 10^{-7} km/s, and particle densities n_0 between 0.1 and 10 cm^{-3} for the initial ISM. Using the relation for R_C of Table 1 and the reference model for normalization, we obtain for the duration needed for the wind: $t_{RG} = const\,[\,R_C^5\, n_0\, v_w^{-2}\, \dot{m}^{-1}\,]^{1/3}$.

We obtain wind durations between 1.3×10^4 and 1.4×10^6 yr prior to the explosion. This provides an upper limit for the duration of the AD disk wind and hence the accretion. Within the picture of an M_{Ch} mass explosion starting from an 0.6 to $1.1 M_\odot$ C/O WD, some $0.7...0.25 M_\odot$ must be accreted. As discussed above, hydrogen is only stable between $2 \times 10^{-8...-6} M_\odot/yr$. Thus, only the long time scale is consistent with a hydrogen accreter. This makes it more likely that the donor was a He star or a C/O accretion disk. Assuming an ISM density of 0.1 to 1 cm^{-3}, between 0.5 and 10 $M_\odot$ would have been swept up by the ISM. We note that, with this constraint, the region within R_2, with $s = 2$ is much too small in all our models (see Table 4). The most likely solution is therefore an AD wind interaction within region II.

For SN 2014J, the following picture emerges as our most likely solution: An enviroment is produced during the RG phase of the WD progenitor, consisting of a low density cavity surrounded by a shell, or a very low density ISM which would obviously not be expected for the starburst galaxy M82. Wind from the accretion disk (AD-wind) runs into this environment and produces a shell structure responsible for the variable narrow lines observed.

Consistent solutions can be obtained if the AD wind interacts either with region I (case A, s=2) or region II (case B, s=0) of the prior RG wind. This wind runs into an ISM of 0.03 and 0.1 cm^{-3}, respectively. The RG winds have a mass loss rate, wind velocity and duration which are 8×10^{-7} $M_\odot/yr$, 30 km/s, 10^6 yr; and 10^{-7} $M_\odot/yr$, 60 km/s and 2×10^6 yr, respectively. For case A, the location of the reversed shock is larger than 20 ly. For case B, the densities in region II are about 0.01 cm^{-3}. Obviously, a lower ISM density by a factor of 10 is a possible solution without the need for an RG wind.

The most likely solutions for case A and B is an AD wind with $(\dot{m}[M_\odot/yr], v_w[km/s])$ of $(10^{-8}, 3000)$ and ($1.5 \times 10^{-8}, 5000$) with a duration t of 35000 yr and 20000 yr, respectively. The inner corresponding void contains $\approx 3.5 \times 10^{-4}$ $M_\odot$ and $\approx 2.9 \times 10^{-4}$ $M_\odot$ of material at a density of $\approx 4 \times 10^{-5}$ and 3×10^{-5} cm^{-3}. The corresponding density is $\sim 4 \times 10^{-5}$ cm^{-3}, the outer shell width is ≈ 2 ly and its density is ~ 0.02 cm^{-3}. For case B, the shell has a thickness of about 2 ly and a density of ≈ 0.03 cm^{-3}. For case A, a thin shell is formed (Fig. 1) with densities decreasing from 10 to 0.1 cm^{-3} over some 0.015 ly. The equivalent width for Na I D is $EW = 27$ mÅ with a velocity dispersion of 14 km/s for case A, and 27 mÅ and 4.2 km/s for case B.

Other analyses of SN 2014J include that of Soker (2015) who concluded that the core-degenerate model alone could account for the observations discussed. Obviously, winds of CDs are a solution among many which may be more favorable because the consistency with other observational properties of SN2014J.

In this context, it may be interesting to apply our method to SN2011fe, one of the best observed SN Ia at a distance of (≈ 6.4 Mpc) (Nugent et al. 2011). This is another nearby, well-observed, very normal SN Ia. Similar to SN 2014J, environmental density constraints have been set for SN2011fe using X-rays by Margutti et al. (2012b) and radio by Chomiuk et al. (2012b). They find upper limits, for a wind CSM environment, of $\dot{m} \lesssim 6 \times 10^{-10} \times v_w/(100\ km/s)\ M_\odot/yr$. For an AD wind of 3000 km/s this limit corresponds to $\dot{m} \lesssim 1.8 \times 10^{-8}$ $M_\odot/yr$. These parameters are consistent with the wind from an accretion disk with a SD progenitors as discussed above. For constant CSM environment, Chomiuk et al. (2012b) found $n_0 \lesssim 6$ cm^{-3} which is above typical density found in our models within the bubble.

Unlike for SN 2014J, no time varying narrow lines have been observed for this event (Patat et al. 2013), which prevents us from specifying shell velocities or distances in conducting our analysis. The narrow lines may either attributed to the ISM or distances significantly larger than in SN 2014J which remains unaffected by the light front (see e.g. Fig. 5 in Graham et al. (2015b)). If there is a shell produced in a CSM, the bubble must be larger than $\gtrsim 40$ ly. For typical AD wind parameters and a constant density environment of 1 cm^{-3}, this requires durations of $t \gtrsim 10^6$ yr or an environment produced by prior mass loss and a duration larger than in SN02014J by a factor of 2 to 4.

4. DISCUSSION AND CONCLUSIONS

We presented theoretical, semi-analytic models for the interaction of stellar winds with the ISM and its implementation in our code SPICE [4]. We assumed spherical symmetry and power-law ambient density profiles. Our free parameters are: the a) mass loss $\dot{m}$, b) wind velocity v_w, c) the particle density n_0 of the in case of a constant density ISM or the mass loss and wind velocity for environments produced by a prior stellar wind, and d) the duration of the wind from the progenitor system.

Our approach provides an efficient method to study a wide range of parameters well beyond what is feasible with complex numerical simulations. Using the Π-theorem allows us to test a wide variety of configurations, properties of the solutions along with their sensitivity and dependencies on the wind and environment parameters. Using these dependencies, we showed how to use observations to find possible solutions. The formalism presented and SPICE may be used for a wide variety of objects, including stellar winds. The speed of the semi-analytic approach produces solutions with low computational overhead. This allows us to evaluate a large parameter space for individual objects, and to include realistic feedback by many objects in star-formation and galactic large-scale simulations.

Here, the formalism has been applied to study SNe Ia and to constrain the properties of progenitor systems. As discussed in the introduction, SNe Ia may originate from a wide range of scenarios and progenitor channels which lead to an ongoing discussion about the nature of these objects, and their diversity. Most of the channels are not well understood and, thus, our range may be wider than realized in nature.

[4] The code SPICE can be obtained by request

We studied a variety of winds within the scenario of M_{Ch} explosions. The winds may originate from the accretion disk, MS and RG donor star, and over-Eddington accretion of H/He rich matter within this scenario.

The environment considered may be produced by the ISM or may be produced by winds during the stages of the evolution of the progenitor prior to becoming a WD for both double or single degenerate systems. Within the M_{Ch} scenarios, we studied wind from the accretion disk, MS and RG donor stars, and over-Eddington accretion of H/He rich matter within parameters suggested from literature as discussed in Sect. 3.

Within the M_{Ch} explosions, we find that the wind from the accretion disk dominates the environment, or the combined wind from an RG donor and the AD. Such wind leads to a low-density "cocoon" of the order of light years in size. The actual size depends on the duration of the progenitor evolution. The calculations reveal that these cocoons are characterized by interior regions with particle densities often as low as $10^{-4} cm^{-3}$ and which are surrounded by a thin shell. This explains why most SNe Ia appear to explode in low density environment, although SN Ia are observed in the galactic halo, the disk and the bulge. The lack of ongoing interaction in SNe Ia may well be understood in the framework of M_{Ch} mass explosions whether they originate from accretion from a MS, RG, He-star or a tidally disrupted WD. If the wind of the progenitor system interacts with a constant, interstellar medium, we expect narrow lines produced by the shell. Our calculations show shell velocities ranging from 10 to 100 km/s. For the $s = 0$ models, the narrow lines are expected to have an equivalent width of $\approx 100 m$Å and are Doppler shifted by about 10 to 20 km/s (see Tables 3, 4 & 5). In contrast, an environment dominated by a prior stellar wind will result in weaker lines with EW lower by one to two orders of magnitude, i.e. 0.5 to 5 mÅ (see Table 6), which is beyond current observational limits for most SNe Ia. For small cocoons, the narrow lines may show variations in strength and velocity on time scales of months due to the radiation from a SNe Ia. Radiation pressure of the SNe Ia light may accelerate nearby shells (as seen in, e.g. SN1993J).

As a separate effect, the SN ejecta may interact with the shell as discussed in Sect. 1. The outer layers of a SNe Ia expands with velocities of 10 to 30 % of the speed of light and we may expect some interaction on time scales between years and several decades (see Tables 3, 5 & 6). For more details, see Hoeflich et al. (2013); Dragulin (2015). Note the possible implications for SN-remnants and their evolution.

We studied the effect of winds in ultra-low density environments. If there is a long delay time between the formation of the WD and the explosion, the progenitor system may have moved into a low density environment. Within M_{Ch} mass explosions, the size of the "cocoon" will be larger by an order of magnitude and we would neither expect narrow lines nor interaction (Sect. 3.2.1). In general, dynamical mergers are expected to often explode in low density environments due to their long delay times but, also, are unlikely to produce a long-duration wind. Thus, some of these objects are expected to show ongoing interaction for sufficiently large samples of SNe Ia.

A step-by-step scheme has been developed to use the narrow lines for the analysis of SNe Ia progenitors. We applied our models to SN 2014J using both the limits from the X-ray and radio, and the observation of narrow lines (Sect. 3.3), and discussed the allowed range of progenitor properties using the analytic relations (Fig. 17). We found the observations to be consistent with an environment produced by a stellar wind. We applied both our analytic solutions to produce the environment and the wind from the progenitor system. We require an environment which has been created recently with times between 1.3×10^4 and 1.4×10^6 yr prior to the explosion. Within the picture of an M_{Ch} explosion starting from an initial 0.6 to 1.1 $M_\odot$ C/O WD, some 0.7...0.25 $M_\odot$ must be accreted. As discussed in the reviews quoted in the introduction, hydrogen is only stable between $2 \times 10^{-8...-6}$ $M_\odot/yr$. Thus, only the upper limit for the evolutionary times is consistent with a hydrogen accreter. This makes it more likely that the donor was a He star or a C/O accretion disk as a result of a tidally disrupted WD in a DD system. As discussed in the introduction, He-triggered or double degenerate explosions may show winds similar to AD and the M_{Ch} models. However, to build up a sufficiently large a He-layer seems to require low accretion rates inconsistent with the short delay times between the RG phase and the explosion. We note that a future generation of double degenerate models may void this argument.

Our analysis of SN 2014J is consistent with other constraints: No RG donor star has been found (Kelly et al. 2014), optical to MIR light curves and spectra are consistent with an Branch-normal M_{Ch} mass explosion and $0.6 M_\odot$ of ^{56}Ni (Marion et al. 2015; Telesco et al. 2015; Churazov et al. 2014; Diamond et al. 2014; Isern et al. 2014), and the lack of polarization (Patat et al. 2015b).

However, within an increasing number of well observed SNe Ia, it also becomes increasingly obvious that SNe Ia are not "all the same". Our conclusion on SN 2014J should not be generalized. Better observation of narrow line systems are a key to the environment of SNe Ia and the diversity.

Within the class of single degenerate systems we found configurations for SN 2014J which are consistent with both the limits from X-rays and radio and the narrow lines. Our solutions invoke a wind from the accretion disk running into an unusually low density ISM environment, $\lesssim 0.01$ cm^{-3}, or a low density cavity created by a RG wind some $20,000$ to $35,000$ yr prior to the explosion (see Sect. 3.3).

We want to put our findings in context of the possible H_α emission discussed in the introduction. Its detectability depends on the amount of hydrogen, the mechanism of ionization, and the sensitivity and timing of the observations. Possible mechanisms include hard radiation from the shock breakout, ^{56}Ni-decay, surface burning of the WD prior to the explosion, interaction in the forward shock with the CSM, and the reversed shock as a result of the interaction between SN and the CSM. The results are very model dependent with various regimes. Based on ionization calculations and the deflagration model W7 (Nomoto et al. 1984) , Cumming et al. (1996) studied in detail pre-ionization of the progenitor winds by supersoft X-ray sources (Greiner et al. 1991; Rappaport et al. 1994; Kahabka & van den Heuvel

1997) and the H_α emission in the outer supernovae ejecta ionized by the reversed shock interacting with the progenitor wind. They parameterized their study in terms of $\dot{M}/v_w$ $[M_\odot\, yr^{-1}\, km^{-1}\, s]$ with v_w being the progenitor wind velocity. Cumming et al. (1996) put their results into context for the observability of H_α emission for local SNe Ia at distances similar to SN 2014J. For $\dot{M}/v_w \lesssim 1.9 \times 10^{-8}$, supersoft X-ray sources dominate the reversed shock mechanism. We note that the actual flux from supersoft X-ray sources may be significantly lower because of material in the progenitor system (Gerardy et al. 2004). The H_α emission in the reversed shock region depends on the ionization fraction of hydrogen. Cumming et al. (1996) found the ionization fraction less than 0.01, at which the emission becomes inefficient for $\lesssim \dot{M}/v_w = 1.5\times10^{-8}$, and full ionization for $\dot{M}/v_w = 1.5\times10^{-6}$. For local supernovae with a reversed shock in a H-rich region, H_α should be observable in high quality spectra for a RG wind with $\dot{M} \sim 10^{-5}\ M_\odot/yr$ and $v_w = 10\ km/s$. Note that the result of Cumming et al. (1996) is consistent with the finding of Gerardy et al. (2004). Using the observed light curves, Gerardy et al. (2004) put strong limits on the ongoing interaction. Without a strong interaction, there is no reversed shock or too weak of one to ionize hydrogen. We note that the dominance of the ionization mechanism will depend on the class of explosion. For example, excitation by ^{56}Ni-decay or the shock breakout can be expected to be small for deflagration models such as W7 or pulsating delayed-detonation models with a significant C/O shell reducing the γ emission, however the role of ^{56}Ni may become important in double-detonation/HeD explosions which show some ^{56}Ni in the outer layers and may produce He-lines instead (Hoeflich & Khokhlov 1996). For the progenitor wind and environment we found for SN 2014J, we do not expect early, observational H_α emission. The mass loss from ADs is smaller by some 3 to 4 orders of magnitude compared to the limits by Cumming et al. (1996) for local SNe Ia, and the forward shock runs into low density material of some $10^{-3\cdots-4} M_\odot$ in the cavity or the ISM.

However, we may be able to see late-time, narrow H_α emission if the the supernova ejecta runs into the shell of the cavity. Due to the low masses of the cavity, the SN ejecta will remain largely unmodified as it travels through the void and produce H_α emission on impact by both the forward and the reversed shock if we have H in the outer layers of the SN. The velocities of the outer layers are about 1/3 c and, for SN 2014J, we may expect emission in about 50 yr. The impact will be earlier for higher density, more compact shells or shells with inner clumps. While we wait to see hydrodynamic interaction for SN 2014J, we could observe young SN remnants for this signature. One such example is the Branch-normal SNe Ia SN1972E in NGC 5253, 3.3 Mpc away (Kirshner & Oke 1975).

Here, our method has been applied to SNe Ia but studies of other types of stellar explosions, namely core-collapse SNe, and SNe interacting with Wolf-Rayet star mass loss, are under way. SPICE may also be used in modeling other hydrodynamic phenomena and and has the potential to include feedback from stellar winds on a subgrid scale in starformation and large scale galactic evolution simulations.

This brings us also to the limit of our analysis. Although our analytic models provide a practical tool for individual shells or shells from well separated phases of mass loss. In reality, nature may be more complicated. The mass loss can be expected to be time dependent. If an environment is formed by this wind, it will deviate from an r^{-2} law. The mass loss may come in phases, namely brief periods of "superwinds" during the RG phase. Moreover, mass loss from the progenitor system may change over time. In fact, multiple narrow lines have been observed e.g. for SN 2014J (Graham et al. 2015b). However, the narrow lines may be produced both in the vicinity of the SN or at any distance by unrelated clouds in the ISM. Without time evolution of the narrow lines or measurements of dust components, the origin of the systems of narrow lines remain unclear. Obviously, detailed calculations for spectra and light curves are needed to quantify the intensity of the narrow lines.

Moreover, multi-dimensional effects need to be considered for a full analysis, for example in instabilities and mixing, non-symmetric winds, and motion of the progenitor system through the ambient medium. A combination of semi-analytic solutions provide a good starting point for more complex, multi-D calculations with more detailed physics, which are under way, to be presented in forthcoming papers. What role and influence dust may have, especially in the outer layers, is another question deserving close attention.

In light of the wide range of progenitor scenarios and properties of the resulting environment, our approach has been justified in order to find the right ballpark in the vast sea of parameters. In reality, however, multi-dimensional affects such as asymmetric winds will become important, including variable winds. Moreover, proper cooling functions and equation of states for the gas are to be taken into account for detailed analysis of high quality data such as SN 2014J.

Acknowledgments: We would like to thank many colleges, collaborators and the referee for helpful discussions and comments. The work presented in this paper has been supported by the NSF projects AST-1008962, "Interaction of Type Ia Supernovae with their Environment", and AST-0708855, "Three-Dimensional Simulations of Type Ia Supernovae: Constraining Models with Observations". In parts, the results presented have been obtained as part of the PhD thesis of Paul Dragulin at Florida State University.

REFERENCES

Aldering, G., Antilogus, P., Bailey, S., et al. 2006, ApJ, 650, 510
Blondin, S., Prieto, J. L., Patat, F., et al. 2009, ApJ, 693, 207
Bours, M. C. P., Toonen, S., & Nelemans, G. 2013, A&A, 552, A24
Branch, D., Livio, M., Yungelson, L. R., Boffi, F. R., & Baron, E. 1995, PASP, 107, 1019
Buckingham, E. 1914, Physical Review, 4, 345
Burns, C. R., Stritzinger, M., Phillips, M. M., et al. 2014, ApJ, 789, 32
Cardelli, J. A., Clayton, G. C., & Mathis, J. S. 1989, ApJ, 345, 245
Chandra, P., Chevalier, R. A., Irwin, C. M., et al. 2012, ApJ, 750, L2
Chevalier, R. A. 1982, ApJ, 258, 790

Chevalier, R. A., & Fransson, C. 2006, ApJ, 651, 381
Chevalier, R. A., & Imamura, J. N. 1983, ApJ, 270, 554
Chevalier, R. A., & Irwin, C. M. 2012, ApJ, 747, L17
Chieffi, A., Domínguez, I., Limongi, M., & Straniero, O. 2001, ApJ, 554, 1159
Chomiuk, L., Soderberg, A. M., Moe, M., et al. 2012a, ApJ, 750, 164
—. 2012b, ApJ, 750, 164
Chugai, N. N. 1986, Soviet Ast., 30, 563
Chugai, N. N., & Danziger, I. J. 1994, MNRAS, 268, 173
Churazov, E., Sunyaev, R., Isern, J., et al. 2014, Nature, 512, 406
Crotts, A. P. S., & Yourdon, D. 2008, ApJ, 689, 1186
Cumming, R. J., Lundqvist, P., Smith, L. J., Pettini, M., & King, D. L. 1996, MNRAS, 283, 1355
Di Stefano, R., & Kilic, M. 2012, ApJ, 759, 56
Di Stefano, R., Voss, R., & Claeys, J. S. W. 2011, ApJ, 738, L1
Diamond, T., Hoeflich, P., & Gerardy, C. L. 2014, ArXiv e-prints
D'Odorico, S., di Serego Alighieri, S., Pettini, M., et al. 1989, A&A, 215, 21
Dragulin, P. 2015, PhD thesis, Florida State University, Tallahassee
Draine, B. T. 2011, Physics of the Interstellar and Intergalactic Medium
Dwarkadas, V. V., & Chevalier, R. A. 1998, ApJ, 497, 807
Eggleton, P. P. 1983, ApJ, 268, 368
Elias-Rosa, N., Benetti, S., Cappellaro, E., et al. 2006, MNRAS, 369, 1880
Feldman, U., Landi, E., & Schwadron, N. A. 2005, Journal of Geophysical Research (Space Physics), 110, 7109
Ferrière, K. M. 2001, Rev. Mod. Phys., 73, 1031
Fesen, R. A., Høflich, P. A., Hamilton, A. J. S., et al. 2007, ApJ, 658, 396
Fisher, A. K. 2000, PhD thesis, THE UNIVERSITY OF OKLAHOMA
Folatelli, G., Phillips, M. M., Burns, C. R., et al. 2010, AJ, 139, 120
Folatelli, G., Morrell, N., Phillips, M. M., et al. 2013, ApJ, 773, 53
Foley, R. J., Simon, J. D., Burns, C. R., et al. 2012, ApJ, 752, 101
Fransson, C., Ergon, M., Challis, P. J., et al. 2014, ApJ, 797, 118
Gerardy, C., et al. 2003, 607, 391
Gerardy, C. L., Hoeflich, P., Fesen, R. A., et al. 2004, ApJ, 607, 391
Goobar, A. 2008, ApJ, 686, L103
Graham, M. L., Sand, D. J., Zaritsky, D., & Pritchet, C. J. 2015a, ArXiv e-prints
Graham, M. L., Valenti, S., Fulton, B. J., et al. 2015b, ApJ, 801, 136
Greiner, J., Hasinger, G., & Kahabka, P. 1991, A&A, 246, L17
Griv, E., Gedalin, M., & Eichler, D. 2009, AJ, 137, 3520
Hachisu, I., Kato, M., & Nomoto, K. 1996, ApJ, 470, L97
—. 1999, ApJ, 522, 487
—. 2008, ApJ, 679, 1390
Hachisu, I., Kato, M., & Nomoto, K.-i. 2010, in Progenitors and Environments of Stellar Explosions, 56
Hachisu, I., Kato, M., Saio, H., & Nomoto, K. 2012, ApJ, 744, 69
Hamuy, M., Trager, S. C., Pinto, P. A., et al. 2000, AJ, 120, 1479
Han, Z., & Webbink, R. 1999, 349, L17
Hatano, K., Branch, D., Lentz, E. J., et al. 2000, ApJl, 543, L49
Hoeflich, P. 2006, Nuclear Physics A, 777, 579
Hoeflich, P., Dragulin, P., Mitchell, J., et al. 2013, Frontiers of Physics, 8, 144
Hoeflich, P., & Khokhlov, A. 1996, ApJ, 457, 500
Höflich, P. A., Khokhlov, A., & Müller, E. 1997, in NATO ASIC Proc. 486: Thermonuclear Supernovae, ed. P. Ruiz-Lapuente, R. Canal, & J. Isern, 659
Hoyle, F., & Fowler, W. A. 1960, ApJ, 132, 565
Isern, J., Knoedlseder, J., Jean, P., et al. 2014, The Astronomer's Telegram, 6099, 1
Judge, P. G., & Stencel, R. E. 1991, ApJ, 371, 357
Kafka, S., & Honeycutt, R. K. 2004, AJ, 128, 2420
Kahabka, P., & van den Heuvel, E. P. J. 1997, ARA&A, 35, 69
Kasen, D. 2010, ApJ, 708, 1025
Kashi, A., & Soker, N. 2011, MNRAS, 417, 1466
Kawara, K., Hirashita, H., Nozawa, T., et al. 2011, MNRAS, 412, 1070
Kelly, P. L., Fox, O. D., Filippenko, A. V., et al. 2014, ApJ, 790, 3
Kirshner, R. P., & Oke, J. B. 1975, ApJ, 200, 574
Krisciunas, K., Hastings, N. C., Loomis, K., et al. 2000, ApJ, 539, 658
Krisciunas, K., Suntzeff, N. B., Candia, P., et al. 2003, AJ, 125, 166
Kromer, M., Sim, S. A., Fink, M., et al. 2010, ApJ, 719, 1067
Krügel, E. 2015, A&A, 574, A8
Landau, L. D., & Lifshitz, E. M. 1971, The classical theory of fields
Livne, E. 1990, ApJ, 354, L53
Mannucci, F., Della Valle, M., & Panagia, N. 2006, MNRAS, 370, 773
Maoz, D., Mannucci, F., & Nelemans, G. 2014, ARA&A, 52, 107
Margutti, R., Parrent, J., Kamble, A., et al. 2014, ApJ, 790, 52
Margutti, R., Soderberg, A. M., Chomiuk, L., et al. 2012a, ApJ, 751, 134
—. 2012b, ApJ, 751, 134
Marietta, E., Burrows, A., & Fryxell, B. 2000, ApJS, 128, 615
Marion, G. H., Sand, D. J., Hsiao, E. Y., et al. 2015, ApJ, 798, 39
Marsch, E. 2006, Living Reviews in Solar Physics, 3, 1
Moore, K., Townsley, D. M., & Bildsten, L. 2013, ApJ, 776, 97
Noci, G., Kohl, J. L., Antonucci, E., et al. 1997, in ESA Special Publication, Vol. 404, Fifth SOHO Workshop: The Corona and Solar Wind Near Minimum Activity, ed. A. Wilson, 75
Nomoto, K. 1982a, ApJ, 257, 780
—. 1982b, ApJ, 253, 798
Nomoto, K., Saio, H., Kato, M., & Hachisu, I. 2006, ArXiv Astrophysics e-prints
Nomoto, K., Thielemann, F.-K., & Yokoi, K. 1984, ApJ, 286, 644
Nomoto, K., Uenishi, T., Kobayashi, C., et al. 2003, in From Twilight to Highlight: The Physics of Supernovae, ed. W. Hillebrandt & B. Leibundgut, 115
Nordin, J., Østman, L., Goobar, A., et al. 2011, ApJ, 734, 42
Nugent, P. E., et al. 2011, Nature, in press, astro-ph/1110.6201
Osterbrock, D. E., & Ferland, G. J. 2006, Astrophysics of gaseous nebulae and active galactic nuclei
Parker, E. N. 1963, Interplanetary dynamical processes.
Pastorello, A., Benetti, S., Bufano, F., et al. 2011, Astronomische Nachrichten, 332, 266
Patat, F., Chandra, P., Chevalier, R., et al. 2007a, Science, 317, 924
Patat, F., Benetti, S., Justham, S., et al. 2007b, A&A, 474, 931
Patat, F., Cordiner, M. A., Cox, N. L. J., et al. 2013, A&A, 549, A62
Patat, F., Taubenberger, S., Cox, N. L. J., et al. 2015a, A&A, 577, A53
—. 2015b, A&A, 577, A53
Pérez-Torres, M. A., Lundqvist, P., Beswick, R. J., et al. 2014, ApJ, 792, 38
Phillips, M. M., Simon, J. D., Morrell, N., et al. 2013, ApJ, 779, 38
Piersanti, L., Gagliardi, S., Iben, Jr., I., & Tornambé, A. 2003a, ApJ, 598, 1229
—. 2003b, ApJ, 598, 1229
Piersanti, L., Tornambé, A., Straniero, O., & Domìnguez, I. 2009, in American Institute of Physics Conference Series, Vol. 1111, American Institute of Physics Conference Series, ed. G. Giobbi, A. Tornambe, G. Raimondo, M. Limongi, L. A. Antonelli, N. Menci, & E. Brocato, 259–266
Quimby, R., Hoeflich, P., & Wheeler, J. C. 2007a, ApJ, 666, 1083
—. 2007b, ApJ, 666, 1083
Ramstedt, S., Schøier, F. L., & Olofsson, H. 2009, A&A, 499, 515
Rappaport, S., Chiang, E., Kallman, T., & Malina, R. 1994, ApJ, 431, 237
Raymond, J. C., Ghavamian, P., Williams, B. J., et al. 2013, ApJ, 778, 161
Readhead, A. C. S. 1994, ApJ, 426, 51
Reimers, D. 1977, A&A, 61, 217
Rest, A., Suntzeff, N. B., Olsen, K., et al. 2005, Nature, 438, 1132
Rest, A., Matheson, T., Blondin, S., et al. 2008, ApJ, 680, 1137
Ruiter, A. J., Belczynski, K., Sim, S. A., Seitenzahl, I. R., & Kwiatkowski, D. 2014, MNRAS, 440, L101
Sadler, B. 2012, PhD thesis, Florida State University
Sako, M., Bassett, B., Becker, A., et al. 2008, AJ, 135, 348
Schaller, G., Schaerer, D., Meynet, G., & Maeder, A. 1992, A&AS, 96, 269
Schlegel, E. M. 1995, Reports on Progress in Physics, 58, 1375
Schlegel, E. M., & Petre, R. 1993, ApJ, 412, L29

Schmidt, B. P., Kirshner, R. P., Leibundgut, B., et al. 1994, ApJ, 434, L19
Sedov, L. I. 1959, Similarity and Dimensional Methods in Mechanics
Shiga, D. 2007, New Scientist, 1
Silverman, J. M., Vinkó, J., Marion, G. H., et al. 2015, MNRAS, 451, 1973
Slavin, J. D., Dwek, E., & Jones, A. P. 2015, ApJ, 803, 7
Soker, N. 2015, MNRAS, 450, 1333
Spitzer, Jr., L. 1968, Dynamics of Interstellar Matter and the Formation of Stars, ed. B. M. Middlehurst & L. H. Aller (the University of Chicago Press), 1
Starrfield, S., Sparks, W. M., & Truran, J. W. 1985, ApJ, 291, 136
Sternberg, A., Gal-Yam, A., Simon, J. D., et al. 2011, Science, 333, 856
Sugimoto, D., & Nomoto, K. 1980, Space Sci. Rev., 25, 155
Telesco, C. M., Höflich, P., Li, D., et al. 2015, ApJ, 798, 93
Tsebrenko, D., & Soker, N. 2015, MNRAS, 447, 2568
van den Heuvel, E. P. J., Bhattacharya, D., Nomoto, K., & Rappaport, S. A. 1992, A&A, 262, 97
Wang, B., Chen, X., Meng, X., & Han, Z. 2009a, ApJ, 701, 1540
Wang, B., & Han, Z. 2012, New A Rev., 56, 122
Wang, B., Meng, X., Chen, X., & Han, Z. 2009b, MNRAS, 395, 847
Wang, L. 2014, Polarimetry of SN 2014J in M82 as a Probe of Its Dusty Environment, HST Proposal
Wang, L., Hoeflich, P., & Wheeler, J. C. 1997, ApJ, 483, L29
Wang, L., Baade, D., Høflich, P., et al. 2003, ApJ, 591, 1110
Wang, X., Li, W., Filippenko, A. V., et al. 2008, ApJ, 677, 1060
Weaver, R., McCray, R., Castor, J., Shapiro, P., & Moore, R. 1977, ApJ, 218, 377
Whelan, J., & Iben, I. J. 1973, 186, 1007
Wood, B. E., Müller, H.-R., Zank, G. P., & Linsky, J. L. 2002, ApJ, 574, 412
Woosley, S. E., & Kasen, D. 2011, ApJ, 734, 38
Woosley, S. E., & Weaver, T. A. 1994, ApJ, 423, 371
Yaron, O., Prialnik, D., Shara, M. M., & Kovetz, A. 2005, ApJ, 623, 398
Zhou, W.-H., Wang, B., & Zhao, G. 2014, Research in Astronomy and Astrophysics, 14, 1146